CONTENTS

SUMMARY 1 1/A5

INTRODUCTION 1 1/A5

SYMBOLS 3 1/A7

CONDITIONS REQUIRED FOR SELF-IGNITION 4 1/A8
Mixture Temperature 5 1/A9
Mixture Pressure 6 1/A10
Mixture Fuel-Air Equivalence Ratio 7 1/A11
Mixture Residence Time 9 1/A13

SELF-IGNITION POINTS IN SCRAMJET CONFIGURATIONS 10 1/A14
Transverse Fuel-Injection Jets 10 1/A14
Downstream Facing Steps With Transverse Injection (Unswept) 11 1/B1
Strut Base Flow Region (Unswept) 11 1/B1

CORRELATION OF HYDROGEN-AIR IGNITION DATA FOR UNSWEPT GEOMETRY 12 1/B2
Simple Ignition Models 12 1/B2
Correlation Parameters 13 1/B3
Ignition Data 15 1/B5
Discussion of the Correlation 16 1/B6

CORRELATION FOR SWEPT GEOMETRY 20 1/B10
Ignition Data 21 1/B11
Discussion of the Correlation 23 1/B13

CONCLUDING REMARKS 26 1/C2

REFERENCES 28 1/C4

TABLES 31 1/C7

FIGURES 36 1/D3

AUG 2 3 1979

NAS 1.60:1457
COMPLETED

NASA Technical Paper 1457

Criteria for Self-Ignition of Supersonic Hydrogen-Air Mixtures

Paul W. Huber, Charles J. Schexnayder, Jr.,
and Charles R. McClinton

AUGUST 1979

NASA

(58)

NASA Technical Paper 1457

Criteria for Self-Ignition of Supersonic Hydrogen-Air Mixtures

Paul W. Huber, Charles J. Schexnayder, Jr.,
and Charles R. McClinton
Langley Research Center
Hampton, Virginia

National Aeronautics
and Space Administration

**Scientific and Technical
Information Branch**

1979

CONTENTS

SUMMARY 1

INTRODUCTION 1

SYMBOLS 3

CONDITIONS REQUIRED FOR SELF-IGNITION 4
Mixture Temperature 5
Mixture Pressure 6
Mixture Fuel-Air Equivalence Ratio 7
Mixture Residence Time 9

SELF-IGNITION POINTS IN SCRAMJET CONFIGURATIONS 10
Transverse Fuel-Injection Jets 10
Downstream Facing Steps With Transverse Injection (Unswept) 11
Strut Base Flow Region (Unswept) 11

CORRELATION OF HYDROGEN-AIR IGNITION DATA FOR UNSWEPT GEOMETRY 12
Simple Ignition Models 12
Correlation Parameters 13
Ignition Data 15
Discussion of the Correlation 16

CORRELATION FOR SWEPT GEOMETRY 20
Ignition Data 21
Discussion of the Correlation 23

CONCLUDING REMARKS 26

REFERENCES 28

TABLES 31

FIGURES 36

SUMMARY

A correlation of available self-ignition data for supersonic hydrogen-air mixtures in configurations representative of scramjet combustors has been made in terms of a pressure-scale product as a function of combustor entrance stagnation temperature. The correlation was examined in light of simplified ignition-limit models developed by assuming ignition time equal to mixture residence time, and by using a global reaction rate to approximate the finite-rate chemistry. The data and ignition-limit models included cases of injection from transverse fuel jets on walls, transverse fuel jets behind swept and unswept steps, and transverse injection ahead of swept and unswept steps and strut bases.

Although the correlation is based on greatly simplified approximations of a very complex phenomenon, it provides useful insight and guidance for indicating the probability of self-ignition in a variety of possible applications.

Some of the more important indications derived from the correlation are summarized as follows:

(1) For the typical case of fuel stagnation temperature much less than air stagnation temperature, the ignition very likely occurs in those regions where the mixture equivalence ratio is approximately 0.2.

(2) Self-ignition is extremely sensitive to the mixture temperature at the pertinent ignition locations. As a result, wall temperature and recirculation-zone temperature recovery factor have dominant influence on the phenomenon, and it is desirable for both to be as high as possible.

(3) For the typical case of highly cooled walls, the ratio of boundary-layer thickness to jet penetration height, step height, or base half-height has strong influence on ignition since it directly influences recirculation-zone recovery temperature.

(4) The likely regions for self-ignition in the combustor seem to have an order of merit as follows: (a) strut bases and steps where the fuel is injected well upstream, (b) the upstream recirculation regions of strong transverse jets on plane surfaces, (c) behind steps with transverse fuel injection, and (d) bow-shock regions of transverse fuel jets.

INTRODUCTION

The objective of this paper is to define the conditions necessary to accomplish self-ignition (also called autoignition or spontaneous ignition) in combustible mixtures flowing at supersonic velocities in configurations representative of air-breathing propulsion systems for hypersonic flight. An important requirement of combustors for this application is that the mixing, ignition, and

reaction be very rapid, so that excessive length (hence, weight, cooling, drag, etc.) is not required.

There is a great abundance of literature dealing with the problem of ignition and reaction of various fuel-air or fuel-oxygen mixtures at low subsonic velocities and for reactant temperatures at, or a little above, room temperature. There is a much lesser, but significant, amount dealing with these problems at supersonic velocities and the associated higher reactant temperatures. (See ref. 1, e.g.) The supersonic studies show that hydrogen fuel is much more desirable than hydrocarbon fuels from the standpoint of fast reaction rates and high heat release per unit mass, although it is less desirable than some of the others from the standpoint of handling and storage. Although the reaction rates for hydrogen combustion are very fast, a rather high temperature is required for ignition, and for typical supersonic combustor entrance flow conditions the static temperatures are too low to achieve self-ignition in a short flow length (even though the total temperature of the flow may be high enough).

In order to circumvent this problem, one or more of the following possible alternatives must be incorporated:

(1) For testing in ground facilities, it is sometimes possible to temporarily increase the facility gas temperature, or fuel temperature, until ignition is obtained, and then reduce it back and maintain the combustion.[1] A flameholder is required to maintain the combustion at the reduced temperature, and knowledge of those factors which influence self-ignition is useful in understanding flameholders since the factors pertinent to each of these processes are similar.

(2) A separate ignition system, such as a high-pressure hydrogen-oxygen flame ignited with a spark, or a small amount of substance having a low ignition temperature, may be added.

(3) The combustor may be configured to provide regions of higher temperature, higher pressure, or lower velocity, which serve as self-ignition points as well as flameholders. This approach is very desirable for subscale engine tests, since the engine design and test procedures are greatly simplified if separate ignitors and temperature surges can be avoided.

It is the purpose of this paper to define those combinations of gas conditions and configuration parameters which allow for self-ignition (i.e., alternatives 1 and 3 of the preceding paragraph) of supersonic hydrogen-air mixtures in combustors of the type contemplated for hypersonic propulsion systems. To accomplish this objective, correlations are made between the geometry and self-ignition conditions from a variety of published experimental studies as well as some new data, including both swept and unswept configurations.

---

[1]Once ignition has occurred, the chain-carriers which are generated become a source of ignition for the oncoming flow. This, along with some local temperature increase due to the reaction, allows combustion to be maintained after the facility temperature is lowered.

SYMBOLS

A,B,C,D	species concentrations (see eq. (3))
b	strut base half-height, m
c	species concentration (subscript denotes species)
C_p	pressure coefficient $C_{p,n} = \dfrac{\frac{p_n}{p} - 1}{\frac{\gamma}{2} M^2}$ (n = s, j, or B)
c_p	specific heat at constant pressure
d	fuel orifice diameter, m
F_R	recirculation zone temperature recovery factor (see eq. (10))
f	reaction rate coefficient
H	transverse jet penetration height (see fig. 10), m
h	step height, m
k_1, k_2	constants in residence time relations (see fig. 10, eqs. (11a) and (11b))
l_i, l_r	ignition, reaction length, m
M	combustor Mach number
m	mass
p	combustor pressure, atm (1 atm = 101.3 kPa)
q	dynamic pressure, atm
S	distance from step to orifice center line in flow direction, m
T	combustor temperature, K
t	time, sec
u	combustor flow velocity, m/sec
x	any nonreacting collision partner; distance along flow direction, m

γ	ratio of specific heats
δ	boundary-layer thickness, m
Λ	sweep angle, deg
$\tau_i, \tau_r, \tau_{res}$	ignition, reaction, residence times, sec
ϕ	fuel-air equivalence ratio, $\phi = 34.3 \frac{m_f}{m_a}$ (for hydrogen-air)

Subscripts:

a	air
B	behind step or base
b	ahead of base
d	ahead of jet flow field
f	fuel
h	ahead of step
j	in recirculating zone ahead of jet
mix	mixture
R	recovery in recirculation zone
s	behind normal shock
t	total or stagnation
w	wall

CONDITIONS REQUIRED FOR SELF-IGNITION

In order to accomplish self-ignition (and combustion) in a flowing combustible mixture it is necessary that four conditions be properly met; these conditions are the static temperature, static pressure, fuel-air mixture, and the residence time (at these conditions). The degree to which any one condition must be met is, of course, dependent upon the degree to which the others are met. In general, the likelihood of ignition and combustion increases as temperature increases, as residence time increases, as the mixture fuel-air equivalence ratio approaches the stoichiometric value, and as pressure increases (within specified limits). These trends are discussed for hydrogen-air in the

following sections where, for simplicity, the chemical-kinetics system for ignition is treated in global fashion, as was done in reference 2 (i.e., an eight-reaction system, given in table I of present paper, was represented by a single hypothetical reaction whose rate variation with temperature and pressure was roughly the same as that of the complete system).

The use of such a global approach (within specified limits) is valid for this study when one examines the curves in figures 1 and 2. Note that the global model was originally developed on the basis of an eight-reaction, six-species chemistry system (table I, ref. 2). The expanded chemistry model is based on many more reactions and species than this, and includes the presently accepted rate values; it should thus represent a good standard for comparison. Figure 1 shows the effect of pressure on ignition time. The dashed curves represent the global approximation (ref. 2), and the solid curves represent an expanded chemistry model (similar to hydrogen-oxygen model in ref. 3) which includes HO_2 and H_2O_2 species and the reactions associated with them. For temperatures above 1000 K, a valid pressure range of 0.2 to 2 atm is indicated. At temperatures less than 1000 K, the solid curves in figure 1 indicate the ignition times increase for a pressure range 1 to 2 atm (1000 K) and for 0.4 to 1 atm (910 K). The author of reference 2 quoted a low temperature limit of 1000 K, which is reasonable for an eight-reaction chemistry model. However, the upper pressure limit at that temperature should be 1 atm instead of the 5 atm given. An upper limit of 5 atm would not apply unless the temperature was 1500 K or greater. Figure 2 shows the effect of equivalence ratio on ignition time. The global approximation assumes a constant ignition time over a range of ϕ from 0.4 to 2, which is reasonable (20-percent error) when compared with the expanded chemistry model curve and theoretical results from references 4, 5, and 6, along with experimental results from reference 7 as reported in reference 4.

Mixture Temperature

If the pressure and fuel-air mixture are held constant, the effect of temperature on ignition (and reaction) time can be readily shown for the global approximation of reference 2 in a plot such as figure 3. Ignition is considered accomplished when the temperature rise reaches 5 percent of the complete reaction temperature rise. In terms of the chemical system, this means that sufficient free radicals, or chain-carriers (i.e., OH, H, and O species which are used over and over to maintain the ignition process), are formed to initiate the reaction system but no appreciable heat is released (formation of the chain-carriers does not involve a significant exothermicity). The reaction time τ_r is defined as that required from ignition until 95 percent of the heat is released (due to formation of the product, H_2O). Note that the ignition time has a strong exponential dependence on temperature, but the reaction time is dependent on temperature to a much lesser extent. Over the range from 1000 K to 2000 K, τ_i varies by about a factor of 100, while τ_r varies by only about a factor of 3 at constant pressure. The following equations for the variation of τ_i and τ_r, respectively, with temperature and pressure are taken from reference 2:

$$\tau_i = \frac{l_i}{u} = \frac{8 \times 10^{-9} e^{9600/T}}{p} \tag{1}$$

$$\tau_r = \frac{l_r}{u} = \frac{0.000105 e^{-1.12T/1000}}{p^{1.7}} \tag{2}$$

The basic reason that τ_i for hydrogen-air has such a strong nonlinear variation with temperature, particularly in the lower part of the range, is that the colliding reactants must possess an energy sufficient to overcome the activation energy required for starting the chain reactions. When the energy level of the reactants is near this minimum value, the probability for ignition is very low; hence, τ_i approaches very high values. At temperatures near 800 K (or a little higher, depending on p and ϕ) the ignition time approaches infinity and self-ignition cannot occur. (See refs. 8 and 9.) Once ignited, large activation energies do not exist because highly reactive chain-carriers have already formed; hence, τ_r has a much smaller variation with temperature.

Mixture Pressure

The first-power pressure dependency of τ_i in equation (1) is because the reactions involved in the ignition chemistry involve only two reactants. For example, for the two-body reaction $A + B \xrightarrow{f} C + D$, the fractional change of the concentration of reactant A during a given time increment is proportional to the concentration of reactant B; that is,

$$\frac{dc_A}{c_A} = -f(c_B)\,dt \tag{3}$$

Since the concentration of any constituent at a given temperature is proportional to pressure, the reaction rate (inverse of τ) is proportional to pressure. Thus, the product $p\tau_i$ forms a single curve in figure 3 for all the pressures, and allows the use of the binary scaling law for the ignition conditions of hydrogen-air mixtures. That is, for a given flow velocity and temperature the ignition characteristics of hydrogen-air are the same for different scaled geometries, providing the product of pressure and scale is held constant (since scale is proportional to τ).

Binary scaling does not apply, however, for the reaction time τ_r because the reaction system involves many three-body reactions. Since three-body reaction rates vary as the square of pressure (there would be two species concentrations in the right side of eq. (3)), it would be expected that the pressure

dependency would be somewhere between p and p^2 (in this case, $p^{1.7}$). Because of this, the $p\tau_r$ curves in figure 3 show some pressure dependency.

Mixture Fuel-Air Equivalence Ratio

It was stated previously that the ignition and reaction times taken from reference 2 were not very dependent on ϕ within the specified range of validity. This is, of course, assuming that the mixture temperature is not dependent on ϕ and would apply to cases of premixed hydrogen-air or unmixed cases where the temperature of the injected hydrogen is the same as that of the air. For the more practical case (for scramjet combustors), where relatively cold hydrogen is injected into hot air, there will be a significant variation of temperature with ϕ through the mixing layer. Since the temperature of the mixture is higher on the low equivalence-ratio side of the mixing layer, and since ignition time is a strong function of the mixture temperature, it would be expected that the self-ignition point would be at the lean side of the mixing layer (low ϕ). For example, consider the variation of ignition time with ϕ shown in figure 4 for a premixed hydrogen-air flow at a uniform temperature of 1220 K, a pressure of 1 atm, and a velocity of 1372 m/s (ref. 6). The theoretical $T = 1220$ K solid curve has been extrapolated to ϕ lower than that given in reference 6 by assuming that the lower limit of ignition for this mixture temperature would be at $\phi \approx 0.05$, and at the limit, $\tau_i \to \infty$. This value of ϕ for the lower ignition limit was estimated by extrapolating the lean limit of combustion as a function of temperature given in reference 8 (≈2 percent hydrogen, by volume, at 1220 K).

In order to approximate the variation of temperature with ϕ through a mixing layer of coflowing cold hydrogen and hot air, the following simplified relation was used:

$$T_{mix} \approx T_a - \frac{0.327\phi}{1 + 0.327\phi}(T_a - T_f) \tag{4}$$

and was obtained from the energy balance between the cold fuel and hot air given by equation (5) (neglects heat transfer and dissipation effects); that is,

$$\frac{T_a - T_{mix}}{T_{mix} - T_f} = \frac{m_f}{m_a}\frac{c_{p,f}}{c_{p,a}} \tag{5}$$

where

$$\frac{m_f}{m_a} = 0.0292\phi \tag{6}$$

and

$$\frac{c_{p,f}}{c_{p,a}} \approx 11.2 \tag{7}$$

The ratio of fuel mass (hydrogen) to air mass is given as a function of ϕ in equation (6), and the ratio of fuel and air specific heats is assumed constant in equation (7) at a value approximating a typical cold-hydrogen and hot-air case. In order to modify the curve for $T = 1220$ K (uniform) to the case of $T = T_{mix}(\phi)$, the following simplified approach was used: it was first assumed that the modified curve would have a temperature of 1220 K at $\phi = 0.5$, and that the injected fuel temperature T_f was 250 K (static T for $M \approx 1$ and $T_t = 300$ K); T_a was then found from equation (4) to be 1380 K; using these values of T_a and T_f in equation (4), values of T_{mix} were found at other values of ϕ (from 0.1 to 1.2);[2] for each value of $T_{mix}(\phi)$, corresponding values of τ_i were read from the $p\tau_i$ curve in figure 3 ($p = 1$ atm); the uniform temperature curve was then modified for $T = T_{mix}(\phi)$ using the relation

$$\tau_i(T = T_{mix}) = \tau_i(T = 1220)\left[\frac{\tau_i(T = T_{mix})}{\tau_i(T = 1220)}\right] \tag{8}$$

The information in the bracketed term is from figure 3, and the modified curve is shown in figure 4 with values of T_{mix} shown at representative points along the curve.

Although the method used to show this effect of temperature variation on ignition time through the mixing layer is somewhat crude, quantitatively, the result is nonetheless interesting and quite meaningful, qualitatively. For example, using a finite-rate reaction system that is generally similar, but differs in some details (number of reactions and values for rate constants) from that used in reference 6, calculations of τ_i were made for the T_{mix} dependency on ϕ as shown in figure 4 and were plotted for comparison. Except for a small displacement in τ_i which can be attributed to the difference in chemistry models, the curves are quite similar. The plot indicates very pointedly that self-ignition will likely originate at a point in the mixing layer where ϕ is on the order of 0.2 for the case of cold hydrogen injection in scramjet combustors. For cases where the fuel is heated, but still has a temperature significantly lower than the air temperature, the ignition point is still

---

[2]Computation of T_{mix} from the static temperatures in this manner neglects heat transfer and dissipation effects due to the differences in velocity and density of the fuel and air; similar results would be obtained if the mixing was assumed to occur at the stagnation temperature of the fuel and air and if the mixture was expanded to the flow velocity.

shifted toward the low ϕ side of the mixing layer (but to a lesser degree than for cold fuel; note that the fuel stagnation temperature is not going to be very close to the air stagnation temperature for supersonic combustion, so that this low ϕ ignition result will generally apply).

Some of the implications of the low ϕ self-ignition point in combustors can be seen from the conceptual sketch of a supersonic hydrogen-air mixing layer in figure 5. This represents the mixing layer between parallel streams of cold hydrogen and hot air at the same static pressure (shear layer) and assumes that the lip of the hydrogen injector is thin enough that self-ignition does not occur in the base recirculation region. While a parallel mixing layer is chosen for illustration, the points to be made apply also to other mixing layers such as those around a perpendicular fuel injection jet. At a distance l_i downstream of the beginning of the mixing at the lip, self-ignition will originate in the low ϕ, high T region where τ_i is a minimum, as seen in figure 4. This minimum τ_i region was arbitrarily selected to be a hydrogen mixture of from 3 percent to 17 percent by volume. The flame will then propagate laterally through the mixture at a rate which varies with ϕ and mixture temperature.[3] Because the flame originates well away from the midpoint of the mixing layer, it must thus travel farther to consume the mixture (the combustible mixture is from about 2 percent to 95 percent hydrogen by volume) than if it originated nearer the midpoint of the mixture. This implies a longer combustor in order to accomplish the required heat release when self-ignition is depended upon as in figure 5. An obvious solution to this problem is to provide a separate ignitor at the beginning of the mixing region, or to configure the combustor for a low-velocity, high-temperature and/or pressure self-ignition and flameholding region at the beginning of the mixing region.

It is interesting to note from figure 5 that, even though this is conventionally termed a "diffusion" type flame (where the combustion rate is limited by the rate of turbulent diffusive mixing), the front actually propagates into a premixed (unignited) flow and thereby is basically a heat conduction flame. That is, the propagation rate is determined by the rate of heat conduction from the burned to the unburned gases, which brings the reactants up to a temperature for fast ignition and reaction. (See ref. 10 for a good discussion of heat conduction flames.) Of course, if the chemical kinetics rates are fast (rapid heat release, hence temperature rise), the heat conduction may propagate the flame fast enough so that the combustion process is mixing controlled, and the previously mentioned ignition delay problem would be negligible, but for slower kinetics, the flame may proceed slower than the mixing in the manner described.

Mixture Residence Time

The previously discussed conditions of temperature, pressure, and fuel-air mixture were presented in terms of their effects on ignition and reaction time.

---

[3]Flame speed generally increases as mixture temperature increases and as ϕ approaches 1.5 to 2.0 (see ref. 8); however, data are not available at these high-temperature conditions. Note that mixture temperature decreases as ϕ increases. (See fig. 4.)

For the ignition and reaction to be accomplished within the combustor (so that the heat release can lead to thrust in the subsequent expansion of the products) the combustor must be sized to provide for an amount of residence time which allows for the mixing, ignition, and reaction times. For the high flow velocities pertinent to supersonic combustion, this can mean excessively long combustors if ignition and combustion are to occur at the static temperature and pressure conditions of the flow. To circumvent this problem, combustors are usually configured to provide local regions in the flow where temperature and/or pressure are significantly higher than static so as to reduce the required τ_i. They are also configured to provide regions of low-velocity, recirculating flow which give part of the flow long residence time and serve as ignition sources and flameholders for the main flow.

SELF-IGNITION POINTS IN SCRAMJET CONFIGURATIONS

The points in typical scramjet combustor configurations at which self-ignition is likely to occur are illustrated in the conceptual sketch shown in figure 6. Some of these points are in the region around transverse fuel jets where high temperatures and pressures are obtained behind the jet bow shocks, or where recirculating zones ahead of and behind the bases of the jets provide zones of long residence time and high temperature. Another point is in the region of recirculation behind rearward facing steps (located on fuel-injection struts or on the walls of the combustor) where long residence time and high temperature may be obtained. Others are in the regions at the bases of fuel-injection struts where recirculation zones exist or where fuel may be injected in the stream direction (parallel injection). These points are discussed separately.

Transverse Fuel-Injection Jets

Figure 7 presents a more detailed picture of the flow region in the vicinity of a transverse fuel-injection jet in supersonic flow. The temperature and pressure rises which occur at the bow shock of the jet and in the recirculation regions increase as the airflow Mach number increases, and the residence time (extent) in the recirculating regions increases as the extent of jet penetration increases. (See ref. 11.) The residence time of the fuel-air mixture in the bow-shock region will be very short since the mixture expands around the jet flow field immediately after compression in the bow shock. Of course, larger diameter jets will increase the residence time in proportion to the jet diameter. It is quite possible that, for the higher Mach number flows, ignition can be initiated in this region but immediately quenched, or partially quenched, in the expansion around the jet.

A more likely place for ignition to occur is in the recirculating zone on the upstream side of the fuel jet base flow, although mixtures here may not be as lean as the desired $\phi \approx 0.2$. (See ref. 9.) This likelihood was observed for a slot injector in reference 12. Here the residence time would be much longer than at the bow shock, and the temperature and pressure would be high due to the near-stagnation of the flow. The recirculating zone downstream of the jet base is too fuel-rich for good ignition. This is shown by the composi-

tion measurements of reference 9 for two-dimensional slot injection and by the observations in reference 13 that air injection into this region greatly enhanced the ignition effectiveness of a circular hydrogen fuel jet.

Downstream Facing Steps With Transverse Injection (Unswept)

As shown by the sketch in figure 8, the situation for ignition at transverse jets behind steps may be quite different than for jets alone (on plane surfaces). This difference is primarily because the recirculating zone ahead of the jet is now too rich for good ignition due to the fact that little or no mainstream air is mixed in due to the shielding action of the step. The extent of the shielding action depends upon the location of the jet downstream of the step. If it is much more than a few step heights (say 5 or 6) downstream, then fuel from the jet may not enter the step region and it may act more like a jet on a plate (the step-separated flow may be reattached well ahead of the jet). In reference 14 this was found to be the case when transverse jets were too far aft of the steps. Even though the mixture is too rich in the plane of the jet, this type of configuration can be a good ignition source at points in the separated flow on either side of the jet (top view in fig. 8) where the mixture is leaner (assuming the jets are not too closely spaced). In addition to having the proper mixture at these points, the separated flow behind the step has a long residence time and high temperature. Figure 9, which is taken from the work of reference 14, shows a top view of the ignition and combustion patterns on an unswept fuel-injection strut. There are four transverse hydrogen fuel-injection jets located behind the step and ahead of the base (the bright line is the strut leading edge, the faint line is the trailing edge, and the dark band is the area aft of the step). The combustor Mach number ahead of the strut is 2.7 and the total enthalpy of the flow corresponds to a flight Mach number of about 7. Although it is a little difficult to see clearly on the photograph, it appears that there are two points where ignition may originate: (1) at the bow shocks of the exposed jet flows (or in the upstream separated regions) or (2) behind the step between the jets (as discussed previously). The latter ignition point becomes more visible at the base of the strut where additional residence time in the base recirculation zone allows for improved ignition and combustion (flameholding action).

Strut Base Flow Region (Unswept)

As was pointed out in the previous section, the strut base flow region can be a very likely point of ignition when fuel is injected from upstream transverse injectors and does not ignite, or is only partially ignited at the jets. This is because the fuel and air are at least partially premixed upon arrival at the base, and there may already be some chain-carriers present. When this "active" mixture is then raised in temperature and given long residence time in the base region, ignition and combustion may readily occur. For the case of no transverse injection jets upstream of the base, but injection of fuel in the streamwise direction from jets in the strut base, there are two possible ignition points. The self-ignition may occur downstream of the base in the mixing region between the coflowing jet and main airstream as discussed previously in connection with figure 5. The self-ignition may also occur in the separated

base flow on either side of the jet where the fuel-air mixture may be suitable (providing the jets are not too closely spaced.) Of course, when there is both transverse injection upstream of the base and parallel injection in the base, the ignition source for the parallel jet is likely to be from the upstream combustion or from premixed gases igniting in the base region as discussed previously. Whether or not this would be an advantage would depend on the relative spanwise locations of the transverse and parallel injectors, the upstream location of the transverse jets, and the fuel flow rates. Finally, it should be noted that the case of transverse fuel injection ahead of a step on the combustor wall, such as in reference 15, should be similar (for gaseous fuel injection) to that of injection ahead of the strut base, with the strut plane of symmetry being the downstream wall.

CORRELATION OF HYDROGEN-AIR IGNITION DATA FOR UNSWEPT GEOMETRY

The preceding discussions have necessarily been based on largely qualitative arguments derived from simplified concepts because the types of flow problems pertinent to the ignition and combustion phenomena in scramjet combustors are extremely complex. Analytical methods are available to model the gross aspects of the combustor flows, but it is not presently possible to model the detailed aspects of such three-dimensional flow regions as those around transverse injection jets (fig. 7) and those behind steps and bases with discrete injection points, in which turbulence modeling and finite-rate chemistry must also be included. However, simple conceptual models can be useful in predicting the trends of self-ignition data with the dependent parameters and can thereby serve as guides to interpretation of the data. Such models will therefore be made and compared with experimental ignition data.

Simple Ignition Models

Simple models for four self-ignition regions are made (see fig. 10) based on the assumption that right at the ignition limit, the ignition time based on conditions in the particular region will just equal the residence time of the flow in that region. Using equation (1) for the ignition time, all the models are of the form

$$\tau_{res} = \frac{8 \times 10^{-9} e^{9600/T}}{p} \tag{9}$$

where it is necessary to specify the residence time, pressure, and temperature for each region. For the three recirculation regions, the conditions of temperature and pressure are reasonably uniform in these low-velocity stirred-flow regions, but the flow behind the bow shock starts out at the normal shock conditions and immediately starts expansion around the jet. Ignition must therefore occur early in the mixing region before the gas has expanded much and thereby quenched the chain-carrier formation.

For the upstream recirculation and bow-shock models shown in figures 10(a) and 10(b), the residence time is expressed as a constant k times a characteristic length divided by a characteristic velocity. Since the residence time in these regions is not known, the use of a constant (to be evaluated later) allows for expression of the residence time in terms of a known length and velocity. For the step and base flow models shown in figure 10(c), the residence time is known from the work of reference 16, by assuming that the step height or base half-height for the present two-dimensional case is equivalent to the radius of the axisymmetric base of reference 16.

The temperature used in the three models involving recirculation regions is the recovery temperature inside these regions and involves a factor F_R which is designated a recirculation-zone temperature recovery factor, or

$$T_R = F_R(T_t - T_w) + T_w \tag{10}$$

This recovery factor is not known and will be determined, to first order, from the data comparisons. Note that the recovery factor is normalized to the wall temperature rather than the flow static temperature because, for highly cooled combustor surfaces, the wall temperature is generally below that of the stream static. The temperature used in the bow-shock model $T_{s,mix}$ is the temperature behind the normal shock (at the combustor Mach number ahead of the jet flow field) reduced due to the cooling of the fuel, as was discussed previously, using equation (4) for $\phi \approx 0.2$ and a fuel total temperature of 300 K. This only amounts to about a 3-percent reduction in normal shock temperature.

The pressure in the recirculation region ahead of the transverse jet is assumed to vary with the Mach number ahead of the jet as shown by the $C_{p,j}$ curve in figure 11 for a 15° cone. The basis for this assumption is the general conical shape of the separation zone upstream of a circular transverse jet and the observation from reference 17 that the pressure is generally lower in this zone for a circular jet than for the two-dimensional slot injection case. (See ref. 9.) The pressure used in the bow-shock model is the normal shock pressure, and is plotted ($C_{p,s}$) as a function of Mach number ahead of the jet in figure 11. The pressure in the recirculation zone behind steps and bases was taken from reference 18 and is shown plotted as $C_{p,B}$ versus Mach number ahead of the step or base in figure 11.

Correlation Parameters

It has previously been shown that the dependent parameters for the ignition process include temperature in the pertinent region, the pressure-scale product for the region, and the equivalence ratio. For simplicity, we can eliminate equivalence ratio on the rationale that we are dealing with diffusion flames involving cold fuel and hot air, so that the point of self-ignition is going to usually be at local values of ϕ near 0.2, as discussed earlier. The remaining dependent parameters are a pressure-scale product versus a temperature. The final questions, therefore, concern what temperature and scale are appropriate.

The proper temperature to use is, of course, the temperature of the mixture at the point of ignition, which is either in a recirculation zone, where a recovery temperature applies, or behind a normal shock. The added complication of dealing with mixture temperature can be eliminated on the same grounds as for ϕ, that ignition will usually occur at $\phi \approx 0.2$. Since the recovery temperature for these complex flows with heat and mass transfer is not known, it is deemed expedient and justifiable to use either the total or static temperature of the free-stream combustor flow as the correlation parameter. For convenience the total temperature is used, but it is recognized that the use of any single temperature has its limitations, since the ignition process represents a history of changing flow conditions from the point of injection to the point of ignition. Chain carrier generation can occur to varying degrees throughout this flow history, but will occur much more rapidly when near the recovery conditions at higher temperatures.

The length scales to use in the correlation are the injector orifice diameters, the step heights, and the strut base half-heights, as shown in figure 10. When the appropriate parameters for residence time, pressure, and temperature, as discussed previously and listed in figure 10, are used in equation (9) in the form for correlation, the four ignition-limit models become as follows:

Jet recirculation region

$$p_d d = \frac{8 \times 10^{-9} e^{9600/T_R}\, u_d}{k_1 \dfrac{p_j}{p_d}} \tag{11a}$$

Bow shock

$$p_d d = \frac{8 \times 10^{-9} e^{9600/T_{s,mix}}\, u_s}{k_2 \dfrac{p_s}{p_d}} \tag{11b}$$

Step recirculation region

$$p_h h = \frac{8 \times 10^{-9} e^{9600/T_R}\, u_h}{80 \dfrac{p_B}{p_h}} \tag{11c}$$

Base recirculation region

$$p_b b = \frac{8 \times 10^{-9} e^{9600/T_R} u_b}{80 \frac{p_B}{p_b}} \tag{11d}$$

For use in evaluation of equations (11), typical combustor entrance velocities and Mach numbers are plotted in figure 12 as a function of the free-stream combustor total temperature. These curves represent nominal values for the general class of scramjets.

Ignition Data

The data used in the correlations are taken from references 6, 13, 14, and 19 to 25 (some of the data used are unpublished). The explanation of data symbols and the experimental data are listed in tables II and III, respectively. These are the unclassified data that are available for hydrogen injected into a supersonic airstream (diffusion flames) and include transverse injectors on plates, transverse injectors behind rearward facing steps, and ignition at strut bases (or steps) where transverse injection occurred upstream of the step or base. The unpublished data represent in-house measurements at Langley Research Center for a transverse jet on a wall (G. Y. Anderson) and transverse jets and steps on walls (J. M. Eggers).

There are two general classes of ignition data given in the tables and plotted in the data correlation figures. The data listed by reference number in the tables are from indirect observations; that is, ignition is sensed by pressure, temperature, or heat transfer measuring instruments at discrete locations downstream of the ignition point. The present data (and the data listed as unpublished) are obtained by direct observation (through windows) and are therefore much more comprehensive as to the location and nature of the ignition phenomenon. For the indirect observations, it was not always possible to know at what point the ignition actually occurred. For example, in the case of transverse jets on plates, the ignition might have been at the jet base recirculation region, the bow-shock region, or, in some cases, at some downstream point (ignition delay). For the case of steps with injection, it was not always certain if the ignition was in the step recirculation zone, at the exposed transverse jet, or at some downstream point.

A general description of the phenomenon, based on the visual[4] observations, is briefly summarized as follows: As tunnel temperature is increased from a

---

[4]A pure hydrogen-air flame does not emit light in the visible region of the spectrum, but impurities such as dust provide enough emission for visual observation.

level where no reaction is observed, visible emission first appears in the region immediately downstream of the bow-shock wave. At higher facility temperature, the visible emission grows in intensity and extends downstream in a narrow half-annular mixing layer. However, the light intensity diminishes with downstream distance, which indicates that although ignition is achieved, it is not yet self-sustaining. As facility temperature is increased further, a very intense emission region appears suddenly along the model surface. This region starts ahead of the jet in the upstream recirculation region and continues downstream with increasing intensity. Because this is the lowest temperature at which the observed ignition is self-sustaining, it is used to define the self-ignition limit. This ignition zone is clearly separate, and apparently independent, from that of the bow shock. The preceding sequence of events generally applies also to the case of a transverse jet behind a step. Therefore, the bow-shock, or off-surface, emission is not herein considered as evidence of true ignition at a transverse jet.

In the figure key (table II), the open symbols indicate that there was no evidence of ignition or combustion within the combustor. The half-filled symbols indicate that there was evidence of an ignition delay, and the filled symbols indicate that ignition was observed (but in the case of the indirect observations, not certain at what specific point in the combustor). The flags on a filled symbol indicate that the test was at a limiting condition, that is, the lowest temperature at which ignition could be observed. When the emission was at the bow-shock region only, and not at the surface (due to upstream recirculation-zone ignition), the symbols are crossed rather than filled. For consistency, the same key is used for all the data figures and is shown in table II.

Discussion of the Correlation

Before detailed comparison of data and the models can be made, it is necessary to select appropriate values of the independent parameters F_R and T_w, which are needed to compute T_R (see eq. (10)), and the constants k_1 and k_2, all of which are needed to evaluate equations (11). Since the wall temperatures are not given for the data presented in this correlation, it is assumed that T_w is always in the range 400 K to 800 K. Both temperatures are used since it is believed that they reasonably bracket the actual experimental values. By using these two values of T_w, the general range of the step and base ignition-limit data is compared with the appropriate models (eqs. (11c) and (11d)) in figure 13 with a wide range of assumed F_R's. It is seen from the figure that values of this recirculation-zone temperature-recovery factor of around 0.4 are needed for general agreement between the data and models. Lower values of F_R are not shown, as they would be off the plot.

Several general conclusions are immediately suggested from the cursory comparison of data and models in figure 13. First, the temperature recovery in the recirculating regions behind the steps and bases is apparently quite low. Second, the self-ignition phenomenon is extremely sensitive to recovery temperature, wall temperature, and flow total temperature.

The low value of F_R is consistent with measurements of temperature in the near-wake separated flow regions behind hypersonic cones, wedges, and blunt-nosed bodies given in reference 26. For Reynolds numbers of around 10^6, which correspond to the general range of data herein, values of F_R from about 0.3 to 0.7 are given for wall-temperature ratios T_w/T_t from about 0.1 to 0.6. Therefore, a value of $F_R \approx 0.4$ for $T_w/T_t \approx 0.3$, which corresponds to the mean of the wall-temperature values for the present data, seems quite reasonable. Based on the shape of the temperature profiles reported in reference 26, as well as other near-wake temperature measurements in the literature, a probable temperature profile for the separated recirculating region behind a step or base is shown in figure 14. The temperature is quite uniform throughout a good portion of the region due to the "stirring" nature of the flow, with the temperature value being roughly midway between stagnation and wall temperature. The sharp drop at the dividing streamline is due to the cooling effect of the upstream wall, and, for the step case, the other sharp drop is due to downstream wall cooling. For the case of base flow, shown by the dashed curve, this wall is absent so that the latter drop is not present and the uniform temperature region T_R is at a somewhat higher temperature. If the upstream boundary layer was thicker (or if the wall was cooler) than shown, then the recovery temperature would be lower, for both the step and base cases.

For the model of the transverse jet upstream recirculation region, it is assumed that the F_R values are generally similar to those deduced for the step and base cases. With this assumption, it is then possible to deduce the value of the constant k_1 from comparison of the data and model. For the bow-shock model, the value for k_2 will likewise be deduced from comparison of data and model. It is implicit in this model that the bow shock occurs in the free-stream exposed flow; that is, the penetration is well beyond the boundary layer ($H \gg \delta$) so that wall temperature and recovery factor are not involved and the normal shock temperature is used.

It is recognized that the assumption of a similar F_R in three of the previously mentioned recirculation-zone models is a rather crude one. However, without actual T_w measurements (which would eliminate the necessity to assume a broad range of T_w) it is not possible to resolve the actual influence of such things as boundary-layer thickness on the recovery factor. The effect of some of these things will be inferred, however, from the more detailed comparisons of the individual models with their respective data.

In figure 15, the upstream recirculation and bow-shock models for a transverse jet are compared with self-ignition data. The values of the constants k_1 and k_2 shown are those which give the best general agreement with the data. Since the models are ignition-limit models, it is to be expected that no ignition would occur below and to the left of a curve, and ignition would be expected to occur above and to the right (higher values of pressure-scale and/or temperature). The product of pressure ahead of the jet and orifice diameter is plotted as a function of total temperature. The circles are for orifices on plane surfaces, and the squares are for orifices behind steps. The latter are included in this correlation because ignition in some cases (small steps or large orifices) may result because of the orifice rather than the step.

Examination of the data leads to the conclusion that jets on plane surfaces produce better surface ignition than jets behind steps. The filled circles are found at significantly lower values of $p_d d$ and T_t (i.e., toward lower left of fig. 15) than are the filled squares. This is an indication of better ignition, which is very likely a result of the shielding action of the step against upstream airflow entering the jet recirculation region, which leads to very rich, cool mixtures. Also, the pressure may be lower than in the unshielded case. When comparison of the ignition-limit models with the ignition-limit data (filled, flagged circles) is made, several interesting results are found. First of all, the lowest ignition-limit data (i.e., two points near $T_t = 1800$ K) correlate with both the upstream recirculation model for $T_w = 400$ K and $F_R = 0.50$ and the bow-shock model for $k_2 = 0.10$. Of course, for the upstream recirculation model, other combinations of T_w and F_R would do almost as well (for example, $T_w = 600$ K and $F_R = 0.45$). Although the best combination of k_1 and F_R cannot be resolved until wall-temperature measurements are available, the models do allow for qualitative comparisons and for good indications of trends with the pertinent parameters. For example, it was previously pointed out that the boundary-layer thickness will influence F_R and that this, along with T_w, will have a strong influence on T_R, and hence on self-ignition. This influence suggests that (1) a transverse jet, step, or base located on a strut mounted in the flow, because of the thinner boundary layer (smaller ratio of δ to H, h, or b), would provide better self-ignition than when located on a wall of the combustor, and (2) an increase in the penetration height of a transverse jet (H in fig. 10) would improve ignition because, according to the results of reference 11, it increases the size of the upstream recirculation zone. This larger recirculation zone would provide a lower value of δ/H, which would increase F_R, and an increased residence time. The penetration of an unconfined jet can be increased by increasing orifice diameter or injection pressure as shown by the following equation from reference 11:

$$H \propto d\left(\frac{q_f}{q_a}\right)^{1/2} \tag{12}$$

Some of these influences on ignition can be seen from the data. For example, the ignition-limit point at $T_t = 1993$ K and $p_d d = 2.75$ (fig. 15) is for a heavy, cooled plate mounted flush with the tunnel nozzle. The wall temperature is probably lower for this point than for the other two ignition-limit points. Also, the three circles at $p_d d = 1.2$ and $T_t = 2130$ to 2415 K are for orifices with smaller diameters than the others on the plot, and they were located on a plate mounted flush with the tunnel nozzle. Since both of these factors lead to a larger δ/H and lower F_R, the result is that no surface ignition (from the upstream recirculation zone) is observed. Only bow-shock ignition was observed, and this was at lower values of F_R than the data. Similar comments can be made for the three small circles at $p_d d \approx 2.6$, for which not even bow-shock ignition was observed. These are for a low q_f/q_a ratio and are on a plate mounted flush with the tunnel nozzle, and both factors should lead to higher δ/H values than the other data. The fact that the transverse jet data seem to exhibit a sensitivity to wall effects, along with the fact that jets

close behind steps are less effective than jets alone, suggests that the source of ignition is more likely to be the upstream recirculation region than the bow shock (the bow-shock model does not involve wall effects). Also, it should be noted in figure 15 that the low q_f/q_a points for jets 3h and 5h behind a step (small, filled, flagged squares at T_t = 2224 and 2261 K) gave better ignition than the low q_f/q_a jets alone, which is contrary to the earlier conclusion for high q_f/q_a jets (the bulk of the data). A probable explanation is that, even though the steps degrade the upstream region for the high q_f/q_a jets (which have a relatively large, hot recirculation zone), the interaction of the smaller upstream recirculation zone (which alone is not very effective), with the nearly reattached flow behind the step, acts to increase the overall recirculation extent favorably. This concept is shown in sketch (a). Of

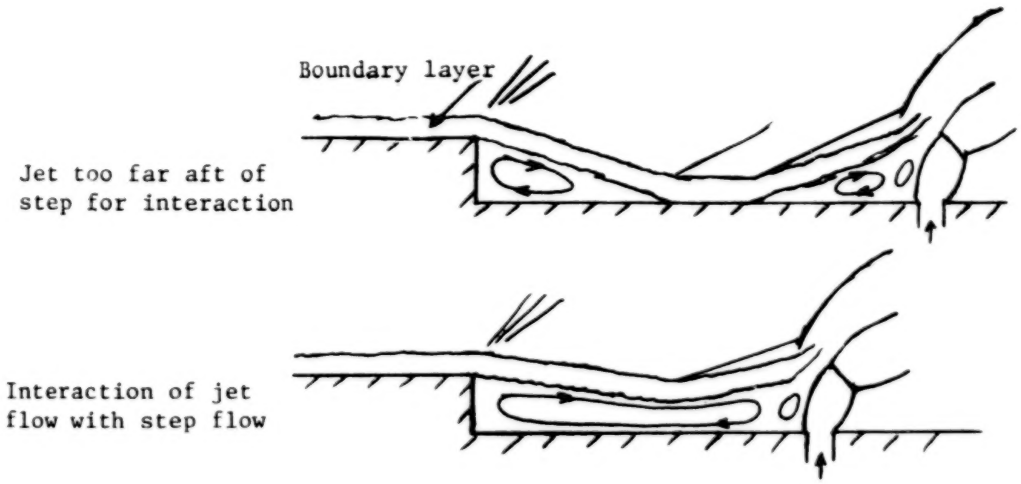

Sketch (a)

course, for other ratios of δ/H, the nature of these effects may be different. It is also interesting to recall that, even though the downstream jet recirculation region is normally too rich to be a good ignition source (ref. 9), it was shown in reference 13 that introduction of an air bleed into the region could result in very good ignition characteristics. With proper modification of the configuration to provide air bleed, this region may then be considered as a likely ignition source.

The product of pressure ahead of a step and step height is plotted in figure 16, and again the squares denote steps with transverse injection behind the steps. These data also show qualitatively the strong sensitivity of ignition to wall temperature and recovery factor indicated by the model. For example, the seven data points shown for $p_h h < 1$ are for uncooled walls which have considerably higher temperatures than those of the other data, especially the points plotted at $T_t < 2200$ K. The point at T_t = 2078 ($p_h h$ = 1.78) is also for a higher temperature wall, but does not represent an ignition limit. The other data involve cooled walls and struts (the strut data are shown with tails). It is interesting to note, for example, that the ignition-limit data (flagged symbols) at the higher values of $p_h h$ and T_t, which indicate poorer ignition characteristics, are for cooled walls. It should also be noted that the two

strut points show somewhat better ignition characteristics than the wall points, even though they do not represent ignition-limit conditions. This improvement may be due to the thinner boundary layer on the struts (lower δ/h, higher F_R) than for the wall data. Finally, it is noteworthy that the data for steps on walls with jets located 5h behind the steps produced surface ignition at the steps (observed visually). In reference 14, however, jets located 5h behind a step on a strut did not produce step ignition, even though the orifices were larger than for the wall cases. This difference may be due to the larger value of δ/h for the wall case, which may lead to greater interaction between the step recirculation zone and the jet upstream zone. That is, for a thin boundary layer, it may be that reattachment takes place behind the step and ahead of the jet upstream recirculation zone. (See sketch (a) on preceding page.)

The product of pressure ahead of a strut base and base half-height is plotted in figure 17. The triangles denote strut bases with transverse injection upstream of the base (triangles can also represent a step on a combustor wall with upstream injection). The ignition-limit model for the base recirculation zone is also plotted in figure 17. There are only three ignition-limit data points (flagged triangles) shown. The two at the higher values of $p_b b$ are for cooled walls, and the point at the lower value of $p_b b$ is for an uncooled strut-type configuration. (The other low $p_b b$ point is also an uncooled case.) The reason for the large uncertainty in plotting the latter point is that there was a broad range of tunnel temperatures covered, but the reference did not identify the conditions at which the ignition was actually observed. The same is true of the point at a lower value of $p_d d$ shown in figure 15. It should be pointed out that the three filled points near $T_t = 2100$ K and $p_b b = 1.5$, as well as the two filled points at $T_t = 1670$ K, are for configurations where there was an upstream step with conditions much more suitable for ignition (much higher pressure-scale product) than at the base. Therefore, these may not be actual self-ignition data.

It can be seen from the comparison of the base data in figure 17 with the transverse injection and step data in figures 15 and 16 that ignition is shown at lower values of pressure-scale product and total temperature (more to the lower left) for the base case. Although these data are too limited to draw any firm conclusions, the apparent improvement in ignition for the base case may be due to (1) a higher recovery temperature caused by the absence of the downstream wall, (2) a leaner (and hence, hotter) mixture, and (3) the presence of chain-carriers from the upstream step injection.

CORRELATION FOR SWEPT GEOMETRY

It was shown in reference 27 that a scramjet with swept geometry can be very advantageous, relative to unswept geometry, in improving engine operational characteristics over a range of flight Mach numbers. However, results of tests of a swept-strut fuel injector (with a step) in reference 28, along with tests of a swept step on a wall and tests of two complete engine configurations (ref. 29), have suggested that the ignition characteristics for swept configurations may be different than those for the unswept case. These probable differences are examined herein.

Ignition Data

Ignition data for the previously mentioned swept-geometry cases, along with data from reference 30 (which is the earliest swept-geometry data), are given in table IV. In order to illustrate the nature of the questions which arose in the tests of the swept configurations, the tests of the instream-mounted fuel-injection strut of reference 28 (Cu strut) will be briefly reviewed.

The Cu strut tests were a follow-on (at $M = 2.2$) to those earlier tests (ref. 30) of an Fe strut at $M = 1.3$ and 1.7. With the low Mach number Fe strut it was found that the minimum stagnation temperature for self-ignition was about 1170 K. Although no tests were conducted at higher temperatures, it was found that combustion was maintained when the temperature was lowered (after ignition) by at least 200 K. It was found in the $M = 2.2$ Cu strut tests that, again, ignition occurred at about 1170 K. No tests were conducted at lower temperatures than this, but it was found that, when the temperature was increased above the minimum for ignition, or when the fuel flow was changed, the streamwise pressure distribution exhibited an anomalous behavior. It no longer exhibited a pressure rise immediately after (or right at) the step as is expected when heat release occurs, but instead showed an expansion followed by a strong pressure rise somewhere along the strut, depending on the tunnel temperature increase and jet fuel flow. At the highest tunnel temperature, the pressure rise occurred at, or aft of, the strut base. (See sketch (b), which shows the pressure distribution along the Cu strut for $M = 2.2$.)

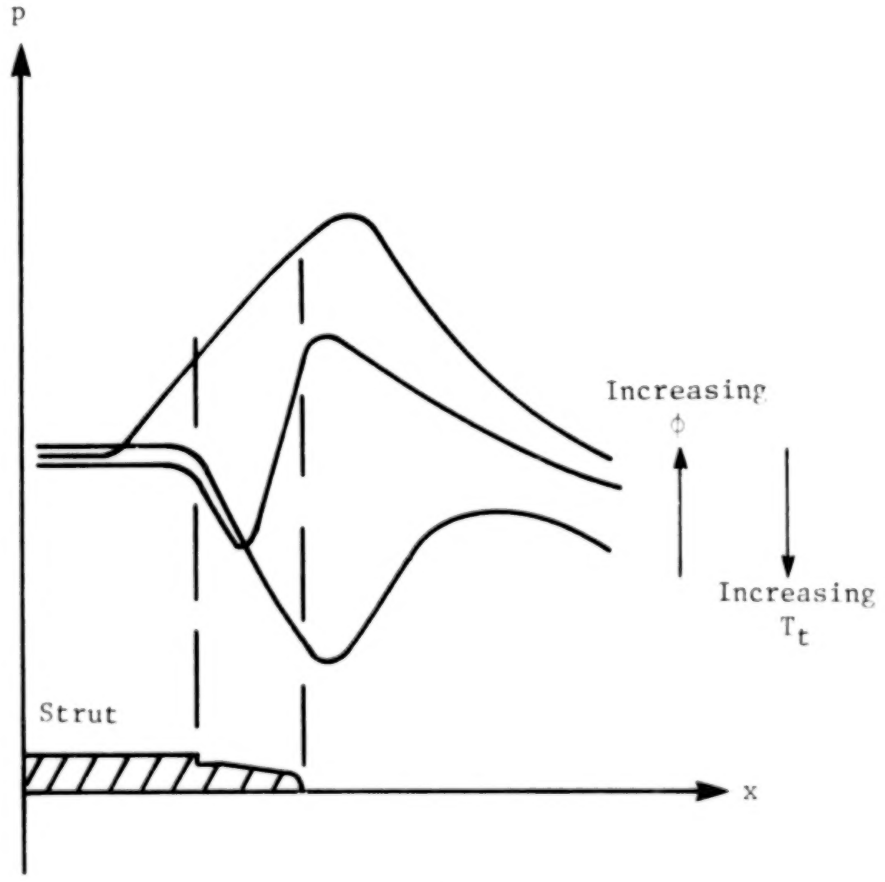

Sketch (b)

The following explanation for the anomalous behavior is proposed: Ignition did not occur at the step or transverse jet, but chain-carriers began to build in concentration at this point and continued to increase as the flow approached the strut base region (as the mixing continued). When this premixed, "activated" gas was brought to recovery temperature and stagnated in the large base recirculation zone, a very sudden ignition occurred along with rapid reaction and heat release. A strong pressure rise therefore occurred at this location (due to the sudden heat release) and the strength of the rise was proportional to the ratio of enthalpy increase due to combustion to the oncoming tunnel flow enthalpy. That is, the pressure rise increased with ϕ and with a decrease of T_t. The sharp pressure rise then caused the boundary layer on the rearward 6^o diverging surface of the strut to separate forward of its normal separation point at the strut base (the new point of separation was dependent upon the pressure rise). Therefore, even though the ignition and heat release occurred at the strut base, and not forward of this point, the effects on pressure distribution were manifested well forward on the strut through the subsonic flow of the separated region of the boundary layer. Of course, the preceding sequence of events happened very fast, so that in a test made at low values of T, or high values of ϕ, it appeared as though the pressure rise originated in the step region (as would be expected if ignition occurred there).

There are a number of factors which make it unlikely that the ignition actually occurred in the step region, or behind the strong pressure front located on the strut (both of these regions are, however, very likely points for the beginning of significant chain-carrier concentration increases). First, and most important, is the fact that if ignition was indeed occurring in the step region at the lower tunnel temperature, then it would be very difficult to explain why a temperature increase, accompanied by a pressure increase (a characteristic of the tunnel operational mode), would not cause the ignition and reaction to be maintained even better than before at the step.[5] The increase in temperature and pressure should have a much stronger positive influence on ignition than the lesser negative influence of velocity increase. This was verified by in-house ignition tests of an unswept step on a wall, where the phenomenon could be observed through a window. When ignition was established at the step, the tunnel temperature (and velocity) was increased, and ignition and reaction were more intense and stable. Furthermore, if ignition and some reaction were occurring at the step, there would be a temperature increase in the recirculating flow, as well as an increase in wall temperature. Both of these factors lead to an increased ignition and flameholding ability and are the reasons why test-gas temperature can generally be reduced (after ignition) and still maintain the ignition and flameholding action of the step. It is, therefore, quite probable that self-ignition and heat release occurred at the strut base rather than at the step or along the strut.

In view of the similarities of this strut and that of reference 30 and their respective test results at 1170 K, it is believed that the same comment

---

[5]The increase in T and p resulted in a somewhat decreased density, so that the resulting change in Reynolds number is not in a direction which causes a downstream movement of separation.

may apply to the low Mach number Fe strut case. It would have been interesting to compare results if the Fe strut had been run at higher temperatures. It is possible, of course, that the surface of the Fe strut may have heated up more than that of the Cu strut enough to make significant differences in the relative ignition behavior. In any event, a one-to-one comparison is not possible because of other differences between the two struts (different Mach number and lateral equivalence ratio). Because of the similarities of all the swept-geometry test configurations listed in table IV with regard to the location of the transverse jet relative to the step, it is assumed that ignition occurred only at the strut base in each case (for the present data, which was not a strut case, no ignition occurred at the step). Using this assumption, only a base flow correlation plot is required (since there is no ignition data for the step and jet) and this is shown in figure 18, where the product of base pressure and base half-height is used. The ignition-limit model is the same as was used for the unswept base flow. Some consideration was given to the use of a swept model, wherein recovery temperature is based on the normal component of velocity ahead of the base, rather than on the streamwise component (which would then be equivalent to an unswept flow with much lower temperature in the recirculation zone). This was not done for several reasons. Among these are: (1) When the normal component of velocity is used, the low-temperature data for the Fe and Cu struts (1010 and 1140 K) would then represent ignition temperatures of 828 and 887 K, respectively, even for $F_R = 1.0$ and no cooling by the fuel. This is too low for physical reality, because at these temperatures the ignition delay time approaches infinity. (2) To say that only the normal component of the stream is recovered behind the base is to say that the cross flow behind the base is equal to the parallel component of the flow ahead of the base. This is also unrealistic since this component is supersonic and the viscous nature of the recirculation zone would certainly reduce this down to low subsonic cross flow.

Discussion of the Correlation

Before comparing the base data with the ignition-limit model as presented in figure 18, it would be well to consider some of the possible reasons for the swept step with transverse injection not producing self-ignition (providing the proposed supposition is correct) at flow conditions and injector-step configurations similar to the unswept cases. The primary reason is believed to be that the flow behind the swept step was too fuel-rich for ignition. This is best illustrated by first referring to figure 19(a) for the top view of a transverse injector behind an unswept step. Note that the fuel-rich contours extend out laterally along the step on either side of the jet, but there is an ignitable region farther out, providing, of course, that adjacent holes are not too close. However, if the fuel flow is increased, or if the holes are moved closer to the step, this overly fuel-rich region may extend out enough so as to be halfway to the adjacent holes, thus disallowing step ignition. It was pointed out in the earlier discussion that rather lean mixtures are required for good ignition because of the cooling effect of the fuel. That is, even though the mixture may not be too rich for combustion (limits are wide for hydrogen), the temperature may be too low for self-ignition unless the mixture is lean. For the case of the swept step, therefore, if the holes are located the same distance behind the step in the flow direction (as was indeed the case for the reported data), then

the holes are in fact located closer to the step in a plane normal to the step, and the lateral extent of the fuel-rich region along the step is increased. (See fig. 19(b).) This argument is made with the assumption that the recirculation-zone geometry is not smaller (reattachment point closer to the step) in the plane perpendicular to the step than for the unswept step. Since the recirculation-zone geometry is probably larger (increases as M decreases), the preceding argument is strengthened (i.e., puts the injector farther forward in the recirculation zone). This ignition problem would certainly be helped by moving the holes farther back from the step in the stream direction so as to be at least at the same normal distance as for the unswept step. Of course, this same type problem should exist for the unswept step if the holes are located too close to the step.

Another possible reason for the lack of step-ignition could be the inability to produce as rapid an increase in chain-carrier concentration due to the cross flow in the recirculating region behind the swept step. It was found in reference 28, however, that placing bounding surfaces ("fences") near the injectors in an attempt to reduce the cross flow apparently does not help the swept-step ignition problem. It should be noted, however, that even though ignition may not occur at the step recirculation zone, this zone along with the exposed part of the jet (bow-shock region), can still be an effective source of chain-carrier generation which can promote more rapid ignition at downstream locations such as the strut base. This was suggested as the result of data comparisons in the unswept base case, and figure 18 shows that the ignition-limit data is at significantly lower values of the pressure-scale product and T_t than any of the unswept data, which again suggests that the base flow region is a more favorable self-ignition region than the others. The lack of a downstream wall should allow for better temperature recovery than would be the case for a step (for the same boundary-layer thickness), and the fuel-air mixture may not be as rich and cold as in the upstream step region since there is time for additional hot air to be entrained before reaching the base region. Of course, the possibility for enhanced ignition due to chain-carriers from the upstream injection may only exist when there is no ignition, or only partial ignition, at the upstream point. If combustion is initiated upstream, the presence of the products of combustion may be more detrimental than helpful; however, base ignition is not then needed.

Another, and perhaps more probable, explanation for the ignition data in figure 18 being better than those on the previous figures is that this is all strut data. None of the strut data on the other figures were ignition-limit data, so it may be that this is a vivid illustration of the strong effects of a higher F_R due to a thinner boundary layer, as discussed previously. For example, this ignition-limit data could be correlated with $F_R = 0.75$ and $T_w = 400$ K, or with $F_R = 0.55$ and $T_w = 800$ K.

It should also be pointed out that the lower of the two data points for the $M = 4$ and $M = 7$ engines on figure 18 (filled points at $T_t = 1400$ K and half-filled points at $T_t = 2165$ K) should probably be no-ignition points since they represent a thin center strut, as opposed to the two thick outer struts (represented by the higher of the two data points) where ignition more likely occurred. (See ref. 29 for the strut geometry of the two engines.)

It is interesting to compare the relative merits of transverse jets on plane surfaces, steps with transverse injection, and bases for self-ignition on the basis of the constants (see eqs. (11)) which best correlated the data. These equations can be put in a form where the right-hand sides of the equations will all be essentially the same and the left-hand sides of the equations will be, respectively,

$$k_1 \frac{u}{u_d}\frac{p_j}{p} d, \quad k_2 \frac{u}{u_s}\frac{p_s}{p} d, \quad 80 \frac{u}{u_h}\frac{p_B}{p} h, \quad 80 \frac{u}{u_b}\frac{p_B}{p} b$$

which involve multiplying factors times the jet diameter, step, or base half-height. By using the indicated values of k_1 and k_2 from the correlations, along with nominal values of the other parameters in the preceding relations, the multiplying factors become approximately 35d, 2.6d, 24h, and 24b.

Since the higher the values of these factors, the better the ignition source, this would indicate that the upstream recirculation zone of the jet is best, and the bow shock is a poor last, as self-ignition sources. This order of merit is in agreement with that suggested earlier by the data comparisons, except that the data indicated that the base region is better than the upstream recirculation region of the transverse jet. There are several possible reasons the base region may actually be the better of the two. First, the upstream recirculation region of the jet may not have a mixture as lean as $\phi \approx 0.2$, which would degrade it because of lower temperatures associated with the richer mixtures of cold fuel. In reference 9, the upstream recirculation region ahead of a transverse two-dimensional jet (slot injection) was reported to have mixtures of the order of $\phi \approx 1.0$ or greater. While the mixtures ahead of the circular jet may be leaner than ahead of the slot, it is not likely that they would be that much more so. Second, as previously mentioned, the base region may benefit from the formation of chain-carriers (from the upstream injection) prior to arriving at the base, thereby giving it "extra" residence time. It should also be pointed out that the scale of the upstream recirculation zone is dependent upon the jet dynamic-pressure ratio q_f/q_a in addition to dependence on orifice diameter (see eq. (12)). For simplicity, the q_f/q_a parameter was not included in equation (11a) since most of the data in figure 15 are for values of $q_f/q_a \approx 3$. If $(q_f/q_a)^{1/2}$ were included along with d, then the constant k_1 would be $20/\sqrt{3} = 12$.

The poor last-place ranking of the bow-shock region shown in the preceding paragraph is not quite as bad as it appears, since one must take into account the fact that the appropriate temperature for this model is $T_{s,mix}$, as opposed to T_R for the other three. $T_{s,mix}$ for the normal shock is higher than T_R for the recirculating regions.

Finally, it should be pointed out that while the effects of cold fuel are manifested in several very important ways for the self-ignition problem (i.e., put constraints on the orifice configuration behind steps, constraints on equivalence ratio for good ignition, etc.) the obvious solution of heating the fuel

may not really be so effective in many cases. For example, at a flight Mach number of 7, stagnation temperatures are about 2100 K, but the highest fuel temperatures expected in flight (or from a heater in a ground facility) are about 900 K. This would still limit self-ignition mixtures to lean values. It can be shown, using equation (4) along with the method of finding ϕ for minimum ignition time (fig. 4), that an increase of fuel temperature of 555 K reduces the required air temperature for ignition by only about 83 K. For low flight Mach numbers ($M \approx 4$) where the fuel heating could be more effective, the air temperatures are too low for self-ignition and separate ignitors (or facility temperatures surges) are required.

CONCLUDING REMARKS

A correlation of available self-ignition data for supersonic hydrogen-air mixtures in configurations representative of scramjet combustors has been made in terms of a pressure-scale product as a function of combustor entrance stagnation temperature. The correlation was examined in light of simplified ignition-limit models developed by assuming ignition time equal to mixture residence time, and by using a global reaction rate to approximate the finite-rate chemistry. The data and ignition-limit models included cases of injection from transverse fuel jets on walls, transverse fuel jets behind swept and unswept steps, and transverse injection ahead of swept and unswept steps and strut bases.

Although the correlation is based on greatly simplified approximations of a very complex phenomenon, and therefore has only qualitative value, it provides useful insight and guidance for indicating the relative probability of self-ignition in a variety of possible applications. The likely regions for self-ignition are those regions where the temperature is higher than flow static temperature, where pressure is higher than flow static pressure, where velocity is lower than free-stream combustor velocity, and where mixtures are within combustible limits. These include bow-shock regions of transverse jets, upstream recirculation regions of transverse jets, recirculation regions behind steps with transverse fuel injection, and recirculation regions behind strut bases and steps with injection ahead of the step or base.

Some of the more important indications derived from the correlation can be briefly summarized as follows:

(1) Pressure-scale product as a function of stagnation temperature is a useful correlation format.

(2) For the typical case of fuel stagnation temperature much less than the air stagnation temperature, the ignition probably occurs in those regions of the mixture where equivalence ratio is approximately 0.2 or a little higher.

(3) As expected, self-ignition is extremely sensitive to the mixture temperature at the pertinent ignition locations. As a result, wall temperature and recirculation-zone temperature recovery factor have dominant influence on the phenomenon, and it is desirable for both to be as high as possible.

(4) For the typical case of highly cooled walls, the ratio of boundary-layer thickness to jet penetration height, step height, or base half-height has strong influence on ignition since it directly influences recirculation-zone recovery temperature. Ignition is therefore more likely on struts, where boundary layers are thinner.

Based on these conclusions, the likely locations for self-ignition seem to have an order of merit, for a given wall temperature, as follows:

(1) Most readily for bases and steps where the fuel is injected well upstream, so that significant mixing and chain-carrier formation begins ahead of the ignition point, and where lean mixtures are more probable. Bases are better than steps because of no downstream wall to cool the mixture. Because of the thinner boundary layer, location on a strut is better than on a combustor wall.

(2) Upstream recirculation region of transverse injection jets on plane surfaces, where fuel penetration is very large compared to the boundary layer thickness. Large diameter orifices and high injection pressure favor this condition.

(3) Transverse injection jets located behind steps. Although jets on plane surfaces are better than jets behind steps for the case of large penetration, the opposite may be true for low jet penetration relative to boundary-layer thickness or step height.

(4) Bow-shock region of transverse injection jets.

Langley Research Center
National Aeronautics and Space Administration
Hampton, VA 23665
May 24, 1979

REFERENCES

1. Waltrup, Paul J.; Anderson, Griffin Y.; and Stull, Frank D.: Supersonic Combustion Ramjet (Scramjet) Engine Development in the United States. 3rd International Symposium on Air Breathing Engines - Proceedings (Munich), DGLR-Fachbuch Nr. 6, Mar. 1976, pp. 835-861.

2. Pergament, Harold S.: A Theoretical Analysis of Non-Equilibrium Hydrogen-Air Reactions in Flow Systems. [Preprint] 63113, American Inst. Aeronaut. & Astronaut., Apr. 1963.

3. Bahn, Gilbert S.: Calculations on the Autoignition of Mixtures of Hydrogen and Air. NASA CR-112067, 1972.

4. Momtchiloff, I. N.; Taback, E. D.; and Buswell, R. F.: Kinetics in Hydrogen-Air Flow Systems. I. Calculation of Ignition Delays for Hypersonic Ramjets. Ninth Symposium (International) on Combustion, Academic Press, Inc., 1963, pp. 220-230.

5. Carson, George T., Jr.: Analytical Chemical Kinetic Investigation of the Effects of Oxygen, Hydrogen, and Hydroxyl Radicals on Hydrogen-Air Combustion. NASA TN D-7769, 1974.

6. Engineering Staff: Hypersonic Research Engine Project - Phase II. Chemical Kinetics Study for a Supersonic Combustor Model. Doc. No. AP-70-6319 (Contract NAS1-6666), AiResearch Manufacturing Co., Garrett Corp., May 20, 1970. (Available as NASA CR-66952.)

7. Schott, G. L.; and Kinsey, J. L.: Kinetic Studies of Hydroxyl Radicals in Shock Waves. II. Induction Times in the Hydrogen-Oxygen Reaction. J. Chem. Phys., vol. 29, no. 5, Nov. 1958, pp. 1177-1182.

8. Drell, Isadore L.; and Belles, Frank E.: Survey of Hydrogen Combustion Properties. NACA Rep. 1383, 1958. (Supersedes NACA RM E57D24.)

9. Thayer, William J., III: The Two-Dimensional Separated Flow Region Upstream of Inert and Chemically Reactive Transverse Jets. D1-82-1066, Flight Sci. Lab., Boeing Sci. Res. Lab., Mar. 1971.

10. Lewis, Bernard; and Von Elbe, Guenther: Combustion, Flames and Explosions of Gases. Second ed., Academic Press, Inc., 1961.

11. Cohen, Leonard S.; Coulter, Lawrence J.; and Egan, William J., Jr.: Penetration and Mixing of Multiple Gas Jets Subjected to a Cross Flow. AIAA J., vol. 9, no. 4, Apr. 1971, pp. 718-724.

12. Yoshida, Akira; and Tsuji, Hiroshi: Supersonic Combustion of Hydrogen in a Vitiated Airstream Using Transverse Injection. AIAA J., vol. 15, no. 4, Apr. 1977, pp. 463-464.

13. Bier, K.; Kappler, G.; and Wilhelmi, H.: Influence of the Injection Conditions on the Ignition of Methane and Hydrogen in a Hot Mach 2 Air Stream. AIAA J., vol. 9, no. 9, Sept. 1971, pp. 1865-1866.

14. Anderson, Griffin Y.; and Gooderum, Paul B.: Exploratory Tests of Two Strut Fuel Injectors for Supersonic Combustion. NASA TN D-7581, 1974.

15. Orth, R. C.; and Cameron, J. M.: Flow Immediately Behind a Step in a Simulated Supersonic Combustor. AIAA J., vol. 13, no. 9, Sept. 1975, pp. 1143-1148.

16. Zakkay, Victor; Sinha, Ram; and Medecki, Hector: Residence Time Within a Wake Recirculating Region in an Axisymmetric Supersonic Flow. Astronaut. Acta, vol. 16, no. 4, June 1971, pp. 201-216.

17. Zukoski, Edward E.; and Spaid, Frank W.: Secondary Injection of Gases Into a Supersonic Flow. Jet Propulsion Center, California Inst. Technol., Oct. 1963.

18. Love, Eugene S.: Base Pressure at Supersonic Speeds on Two-Dimensional Airfoils and on Bodies of Revolution With and Without Fins Having Turbulent Boundary Layers. NACA TN 3819, 1957. (Supersedes NACA RM L53C02.)

19. McClinton, C. R.; and Gooderum, P. B.: Direct-Connect Test of a Hydrogen-Fueled Three-Strut Injector for an Integrated Modular Scramjet Engine. 14th JANNAF Combustion Meeting, Volume II, T. W. Christian, ed., CPIA Publ. 292 (Contract N00017-72-C-4401), Appl. Phys. Lab., Johns Hopkins Univ., Dec. 1977, pp. 489-505.

20. Anderson, Griffin Y.; Eggers, James M.; Waltrup, Paul J.; and Orth, Richard C.: Investigation of Step Fuel Injectors for an Integrated Modular Scramjet Engine. 13th JANNAF Combustion Meeting, Volume III, CPIA Publ. 281 (Contract N00017-72-C-4401), Appl. Phys. Lab., Johns Hopkins Univ., Dec. 1976, pp. 175-189.

21. McClinton, Charles R.: Interaction Between Step Fuel Injectors on Opposite Walls in a Supersonic Combustor Model. NASA TP-1174, 1978.

22. Eggers, James M.; Reagon, Patricia G.; and Gooderum, Paul B.: Combustion of Hydrogen in a Two-Dimensional Duct With Step Fuel Injectors. NASA TP-1159, 1978.

23. Russin, Wm. Roger: The Effect of Initial Flow Nonuniformity on Second-Stage Fuel Injection and Combustion in a Supersonic Duct. NASA TM X-72667, 1975.

24. Burnett, Duane; and Czysz, Paul: Supersonic Hydrogen Combustion Studies. ASD-TDR-63-196, U.S. Air Force, Apr. 1963.

25. Rogers, R. C.; and Eggers, J. M.: Supersonic Combustion of Hydrogen Injected Perpendicular to a Ducted Vitiated Airstream. AIAA Paper No. 73-1322, Nov. 1973.

26. Huber, Paul W.; and Hunt, James L.: Reynolds Number Dependence of Apollo Near-Wake Temperature. AIAA J., vol. 6, no. 1, Jan. 1968, pp. 184-185.

27. Henry, John R.; and Anderson, Griffin Y.: Design Considerations for the Airframe-Integrated Scramjet. NASA TM X-2895, 1973.

28. Northam, G. B.; Trexler, C. A.; and Anderson, G. Y.: Characterization of a Swept-Strut Hydrogen Fuel-Injector for Scramjet Applications. 15th JANNAF Combustion Meeting, Volume III, T. W. Christian, ed., CPIA Publ. 297 (Contract N00024-78-C-5384), Appl. Phys. Lab., Johns Hopkins Univ., Feb. 1979, pp. 393-410.

29. Guy, Robert W.; and Mackley, Ernest A.: Initial Wind Tunnel Tests at Mach 4 and 7 of a Hydrogen-Burning, Airframe-Integrated Scramjet. NASA paper presented at the 4th International Symposium on Air Breathing Engines (Lake Buena Vista, Fla.), Apr. 1-6, 1979.

30. Anderson, Griffin Y.; Reagon, Patricia G.; Gooderum, Paul B.; and Russin, W. Roger: Experimental Investigation of a Swept-Strut Fuel-Injector Concept for Scramjet Application. NASA TN D-8454, 1977.

TABLE I.- HYDROGEN-AIR CHEMISTRY MODEL

[From ref. 2]

$H_2 + X \rightleftarrows H + H + X$

$O_2 + X \rightleftarrows O + O + X$

$H_2O + X \rightleftarrows OH + H + X$

$OH + X \rightleftarrows O + H + X$

$O + H_2O \rightleftarrows OH + OH$

$H + H_2O \rightleftarrows OH + H_2$

$H + O_2 \rightleftarrows OH + O$

$O + H_2 \rightleftarrows H + OH$

TABLE II.- EXPLANATION OF DATA SYMBOLS FOR FIGURES 15 TO 18

Low q_f/q_a	High q_f/q_a	
○	◯	Orifices on plane surfaces
□	□	Orifices behind steps
△	△	Bases or steps with upstream injection

Filled symbol - ignition at surface
Half-filled symbol - delayed ignition (occurs downstream)
Open symbol - no ignition anywhere
Flagged symbol - ignition limit
Tailed symbol - strut configuration
Crossed symbol - bow shock emission only (off-surface)
One rudder[a] - 3h behind step
Two rudders[a] - 5h behind step
No rudders[a] - 1 to 2h behind step

[a]Applies to squares only.

TABLE III.- IGNITION DATA FOR UNSWEPT CONFIGURATIONS

Configuration	Source (a)	T_t, K	M	d, mm	h, mm	b, mm	S/h	P_d, atm	P_h, atm	P_b, atm	$P_d d$, atm-mm	$P_h h$, atm-mm	$P_b b$, atm-mm	Data symbols			Remarks
														Fig. 15	Fig. 16	Fig. 17	
Single strut	14	2055	2.4	4.45	1.80	3.18	1.4 3.5	1.0	1.0	1.0	4.45	1.80	3.18	■	■	▲	Cooled Cooled
Three strut	19	2055	2.7	3.05	3.05	2.34	2.1	1.0	1.0	0.55	3.05	3.05	1.29	■	■	▲	Cooled
Stepped injector	20	2110	2.7	5.16	3.81	2.03	2.3	1.1	1.1	0.70	5.68	4.19	1.42	■	■	▲	Heavy wall, uncooled
	20	2110	2.7	5.16	3.81	2.03	2.3	1.1	1.1	0.87 .70	5.68	4.19	1.77 1.42	■	■	▲	Heavy wall, uncooled Heavy wall, uncooled
	21	2110	2.7	2.95	3.81	----	1.0	0.83	0.83	----	2.45	3.16	----	■	■	---	Heavy wall, uncooled
	22	2110	2.7	5.16	3.81	1.6 2.31	1.3 2.3	1.1	1.1	0.87 .70	5.68	4.19	1.39 1.62	■	■	▲	Heavy wall, uncooled Heavy wall, uncooled
	22	2110	2.7	2.79	3.81	1.6 2.31	1.3 2.3	1.1	1.1	0.87 .70	3.07	4.19	1.39 1.62	■	■	▲	Heavy wall, uncooled Heavy wall, uncooled
	22	1670	2.7	5.16	3.81	1.6 2.31	2.3	1.1	1.1	1.00 .90	5.68	4.19	1.6 2.08	■	■	▲	Heavy wall, uncooled Heavy wall, uncooled
	22	1670	2.7	2.79	3.81	1.6 2.31	1.3	1.1	1.1	1.00 .90	3.07	4.19	1.6 2.08	■	■	▲	Heavy wall, uncooled Heavy wall, uncooled
Staged injector	23	1680	2.7	1.80	----	----	---	0.75	----	----	1.35	----	----	○	---	---	First stage
	23	1680	2.7	3.81	----	----	---	0.75	----	----	2.86	----	----	●	---	---	Second stage
	23	2100	2.7	3.81	----	----	---	0.75	----	----	2.86	----	----	●	---	---	Second stage
Single orifice on plate	13	1820 ±85	2.0	1.52	----	----	---	1.0	----	----	1.52	----	----	●	---	---	Uncooled Uncooled
	U	2110	2.7	3.18	----	----	---	1.0	----	----	3.18	----	----	●	---	---	Uncooled
Orifice behind step	U	1720	2.0	0.89	0.84	----	2.0	1.0	1.0	----	0.89	0.84	----	□	□	---	Preheated, uncooled wall
	U	2035	2.0	0.89	0.84	----	2.0	1.0	1.0	----	0.89	0.84	----	◹	◹	---	Preheated, uncooled wall

[a]See footnote at end of table, page 34.

TABLE III.- Continued

Configuration	Source (a)	T_t, K	M	d, mm	h, mm	b, mm	S/h	P_d, atm	P_h, atm	P_b, atm	$P_d d$, atm-mm	$P_h h$, atm-mm	$P_b b$, atm-mm	Data symbols Fig. 15	Data symbols Fig. 16	Data symbols Fig. 17	Remarks
Orifice behind step	U	2169	2.0	0.89	0.84	----	2.0	1.0	1.0	----	0.89	0.84	----	■	■	---	Preheated, uncooled wall
	U	2078	2.0	1.78	1.78	----	2.0	1.0	1.0	----	1.78	1.78	----	■	■	---	Preheated, uncooled wall
Orifice row ahead of step	24	2330 ±275	4.2	2.18	---	4.75	-3.3	0.15 ±.06	---	0.15 ±.06	0.33 ±.13	----	0.71 ±.29	◗	---	▲	Uncooled strut Uncooled strut
Single orifice ahead of step	U	2050	2.0	1.04	---	0.84	-13	1.0	---	1.0	1.04	----	0.84	●	---	▲	Preheated, uncooled
Orifice row on wall	25	2200	2.7	2.08	---	----	-----	1.0	---	----	2.08	----	----	●	---	---	Uncooled
	25	2200	2.7	5.94	---	----	-----	1.0	---	----	5.94	----	----	●	---	---	Uncooled
Orifice row on annular wall	6	1780	2.8	3.02	---	----	-----	0.71	---	----	2.15	----	----	◗	---	---	Highly cooled
Orifices on plate	P	2128	2.7	1.17	---	----	-----	1.01	---	----	1.18	----	----	○	---	---	Uncooled
	P	2280	2.7	1.17	---	----	-----	0.98	---	----	1.15	----	----	⊕	---	---	Uncooled
	P	2413	2.7	1.17	---	----	-----	1.03	---	----	1.21	----	----	⊕	---	---	Uncooled
Orifices ahead of step	P	2080	2.7	2.64	---	3.81	-1.7	1.09	---	1.09	2.87	----	4.15	●	---	▲	Heavy wall, cooled
	P	1993	2.7	2.64	---	3.81	-1.7	1.04	---	1.04	2.75	----	3.97	◗	---	▲	Heavy wall, cooled
	P	1939	2.7	2.64	---	3.81	-1.7	1.01	---	1.01	2.66	----	3.84	⊕	---	△	Heavy wall, cooled
	P	1752	2.7	2.64	---	3.81	-1.7	0.94	---	0.94	2.48	----	3.58	⊕	---	△	Heavy wall, cooled
	P	1993	2.7	2.64	---	3.81	-1.7	0.62	---	0.62	1.64	----	2.36	⊕	---	△	Heavy wall, cooled
	P	1841	2.7	2.64	---	3.81	-1.7	0.56	---	0.56	1.48	----	2.13	⊕	---	△	Heavy wall, cooled
	P	1822	2.7	2.64	---	3.81	-1.7	0.97	---	0.97	2.57	----	3.71	⊕	---	△	Heavy wall, cooled
	P	1667	2.7	2.64	---	3.81	-1.7	0.89	---	0.89	2.35	----	3.40	⊕	---	△	Heavy wall, cooled

[a]See footnote at end of table, page 34.

TABLE III.- Concluded

Configuration	Source (a)	T_t, K	M	d, mm	h, mm	b, mm	S/h	P_d, atm	P_h, atm	P_b, atm	$P_d d$, atm-mm	$P_h h$, atm-mm	$P_b b$, atm-mm	Data symbols			Remarks
														Fig. 15	Fig. 16	Fig. 17	
Orifices ahead of step	P	1593	2.7	2.64	----	3.81	-1.7	0.85	----	0.85	2.24	----	3.24	○	---	△	Heavy wall, cooled
	P	1935	2.7	2.64	----	3.81	-1.7	1.00	----	1.00	2.64	----	3.81	○	---	△	Heavy wall, uncooled, low q_f/q_a
	P	2076	2.7	2.64	----	3.81	-1.7	0.99	----	0.99	2.61	----	3.77	○	---	▲	Heavy wall, uncooled, low q_f/q_a
	P	2261	2.7	2.64	----	3.81	-1.7	0.98	----	0.98	2.59	----	3.73	○	---	▲	Heavy wall, uncooled, low q_f/q_a
Orifices behind step	P	2378	2.7	1.17	0.84	----	3.0	0.95	0.95	----	1.11	0.80	----	■	■	---	Uncooled
	P	2293	2.7	1.17	0.84	----	3.0	0.99	0.99	----	1.16	0.83	----	■	■	---	Uncooled
	P	2324	2.7	1.17	0.84	----	3.0	0.76	0.76	----	0.89	0.64	----	□	□	---	Uncooled
	P	2426	2.7	1.17	0.84	----	3.0	0.73	0.73	----	0.85	0.61	----	■	■	---	Uncooled
	P	2339	2.7	2.64	3.81	----	1.0	0.75	0.75	----	1.98	2.86	----	□	□	---	Heavy wall, cooled
	P	2220	2.7	2.64	3.81	----	1.0	0.77	0.77	----	2.03	2.93	----	□	□	---	Heavy wall, cooled
	P	2413	2.7	2.64	3.81	----	1.0	1.01	1.01	----	2.67	3.85	----	◪	◪	---	Heavy wall, cooled
	P	2022	2.7	2.64	3.81	----	3.0	1.02	1.02	----	2.69	3.89	----	■	■	---	Heavy wall, cooled
	P	2461	2.7	2.64	3.81	----	3.0	0.61	0.61	----	1.62	2.33	----	■	■	---	Heavy wall, cooled
	P	2261	2.7	2.64	3.81	----	3.0	0.99	0.99	----	2.61	3.77	----	■	■	---	Heavy wall, cooled, low q_f/q_a
	P	2174	2.7	2.64	3.81	----	5.0	0.92	0.92	----	2.43	3.51	----	■	■	---	Heavy wall, cooled
	P	2224	2.7	2.64	3.81	----	5.0	1.02	1.02	----	2.69	3.89	----	■	■	---	Heavy wall, cooled, low q_f/q_a

[a]Reference number given for published data; U for unpublished data; P for present data.

TABLE IV.-IGNITION DATA FOR SWEPT CONFIGURATIONS

Configuration	Source (a)	T_t, K	M	d, mm	h, mm	b, mm	S/h	P_d, atm	P_h, atm	P_b, atm	$P_d d$, atm-mm	$P_h h$, atm-mm	$P_b b$, atm-mm	Sweep angle, deg	Data symbols Fig. 18	Remarks
Fe strut	30	1180	1.7	2.01	2.69	6.35	2.9	1.2	1.2	0.55	2.41	3.23	3.51	45	▲	Uncooled, heavy wall
	30	1150	1.3	2.01	2.69	6.35	2.9	3.4	3.4	1.41	6.83	9.14	8.97	45	▲	Uncooled, heavy wall
	30	1010	1.3	2.01	2.69	6.35	2.9	3.4	3.4	1.41	6.83	9.14	8.97	45	▲	Uncooled, heavy wall
Cu strut	28	1140	2.2	3.18	2.74	6.35	1.6	1.2	1.2	0.64	3.81	3.30	4.06	45	▲	Uncooled, heavy wall
	28	1885	2.2	3.18	2.74	6.35	1.6	1.5	1.5	0.80	4.78	4.11	5.08	45	▲	Uncooled, heavy wall
	28	2280	2.2	3.18	2.74	6.35	1.6	1.8	1.8	0.96	5.72	4.93	6.10	45	▲	Uncooled, heavy wall
Step on wall	P	2270	2.7	1.17	0.84	----	3.0	0.88	0.88	----	1.03	0.74	----	40	---	Uncooled
	P	2452	2.7	1.17	0.84	----	3.0	0.87	0.87	----	1.02	0.73	----	40	---	Uncooled
	P	2239	2.7	1.17	0.84	----	3.0	0.99	0.99	----	1.15	0.83	----	40	---	Uncooled
	P	2350	2.7	1.17	0.84	----	3.0	1.02	1.02	----	1.19	0.86	----	40	---	Uncooled
Mach 7 scramjet	29	2165	3.2	1.14	0.84	1.40 2.54	3.0	0.25 .33	0.25 .33	0.15 .20	0.29 .38	0.21 .28	0.21 .51	48	◭	Cooled struts Cooled struts
	29	2165	3.2	1.14	0.84	6.35 9.53	3.0	0.25 .33	0.25 .33	0.10	0.29 .38	0.21 .28	0.64 .95	48	▲	Cooled struts Cooled struts
Mach 4 scramjet	29	1400	2.2	0.84	0.84	1.40 3.05	3.0	1.2	1.2	0.6	1.01	1.01	0.84 1.83	48	▲	Uncooled struts Uncooled struts
	29	1220	2.2	0.84	0.84	1.40 3.05	3.0	1.2	1.2	0.6	1.01	1.01	0.84 1.83	48	△	Uncooled struts Uncooled struts

[a]Reference number given for published data; P for present data.

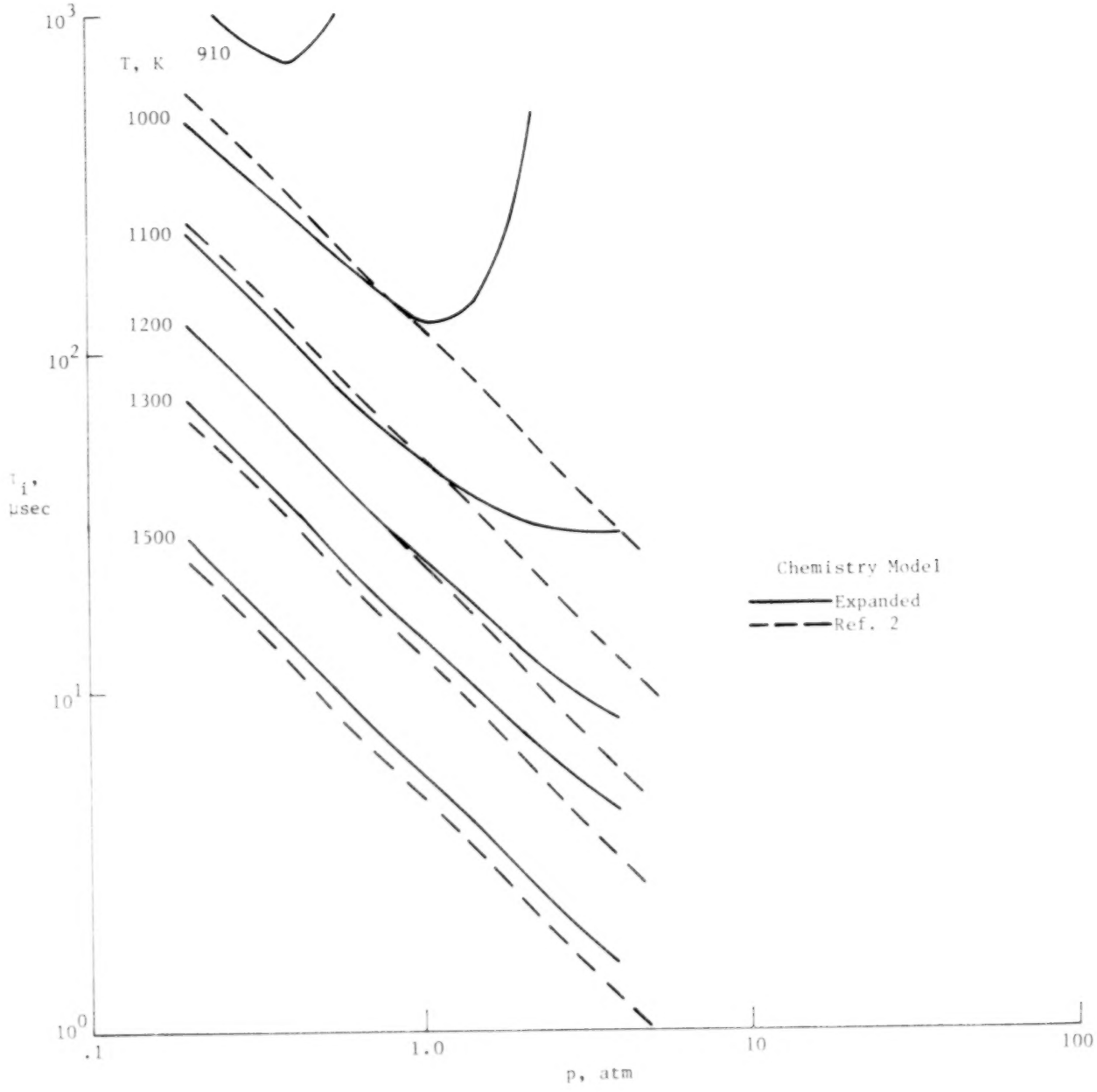

Figure 1.- Effect of pressure on ignition time (hydrogen-air; $\phi = 1$).

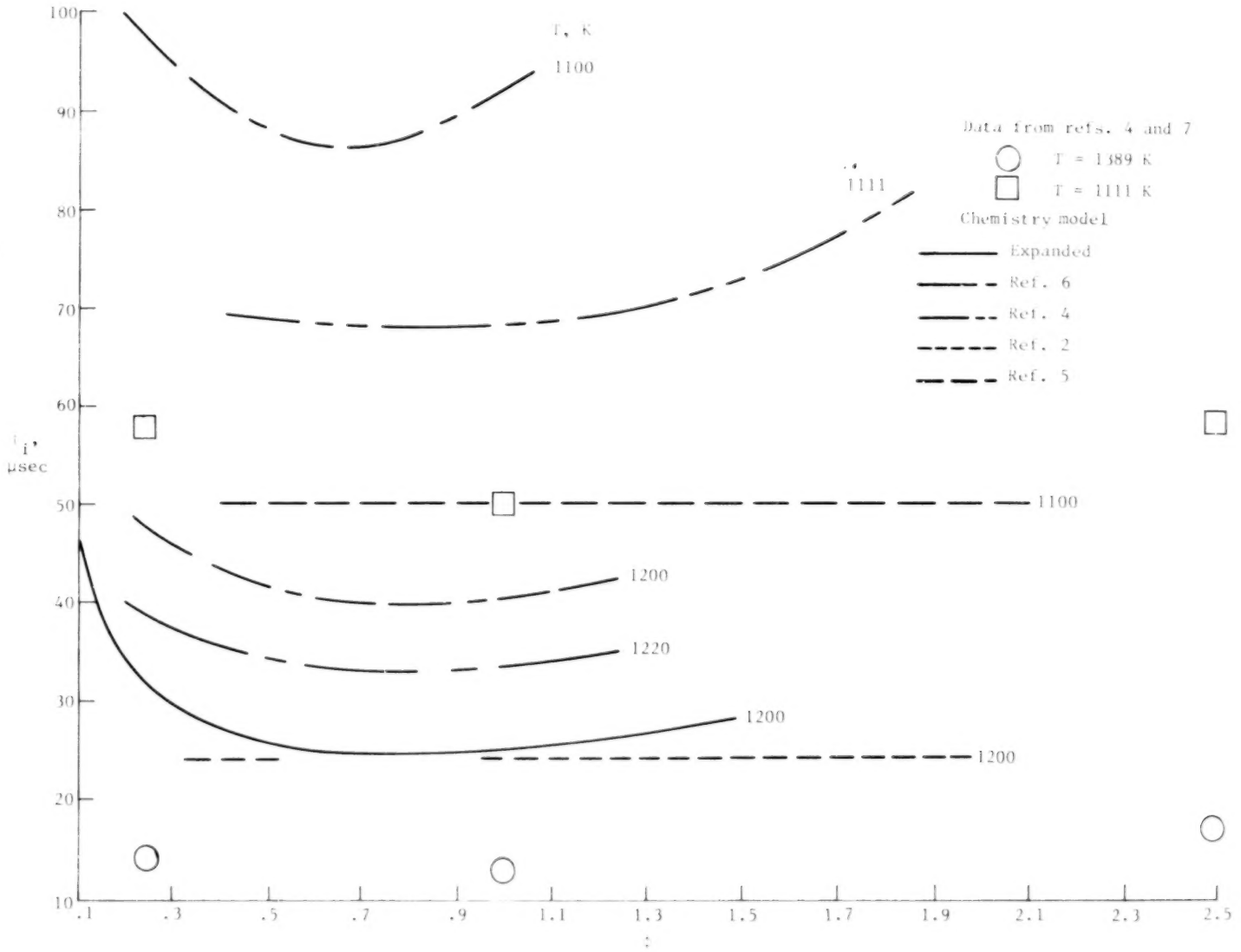

Figure 2.- Effect of equivalence ratio on ignition time (hydrogen-air; p = 1 atm).

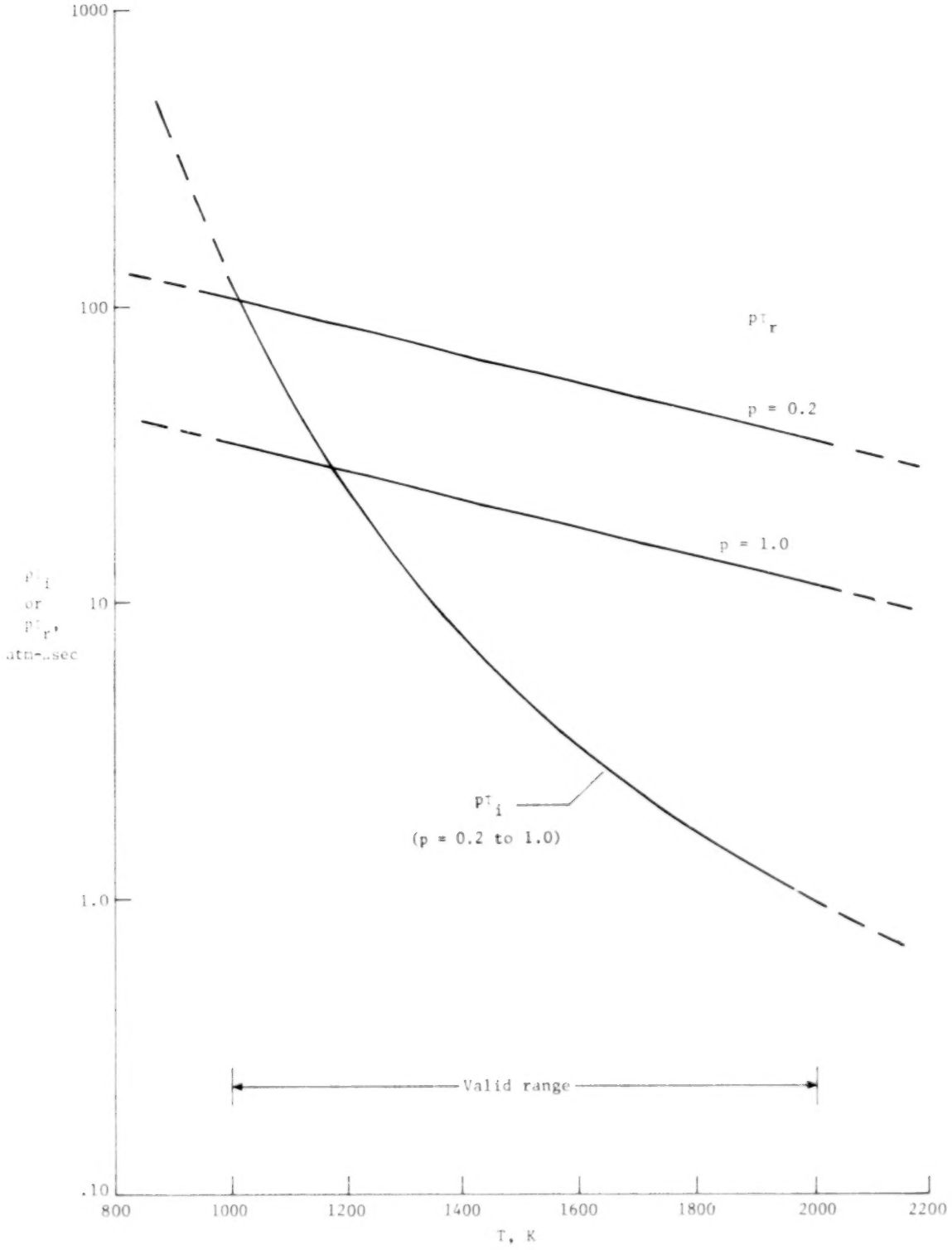

Figure 3.- Variation of ignition and reaction times with temperature and pressure for H_2 - air mixtures (from ref. 2).

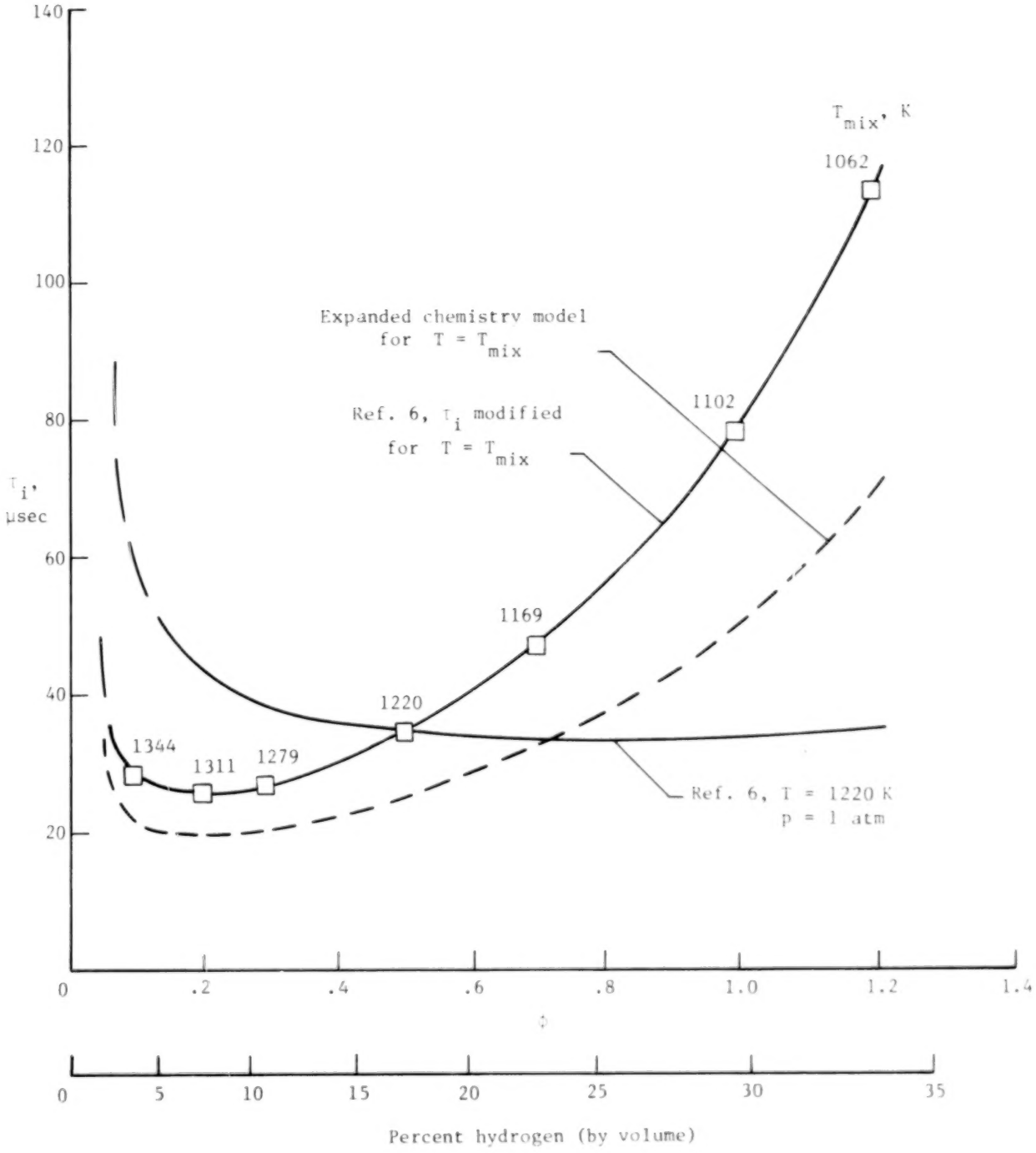

Figure 4.- Variation of ignition time with fuel-air equivalence ratio for cold H_2 injected into hot air. T_a = 1380 K; T_f = 250 K.

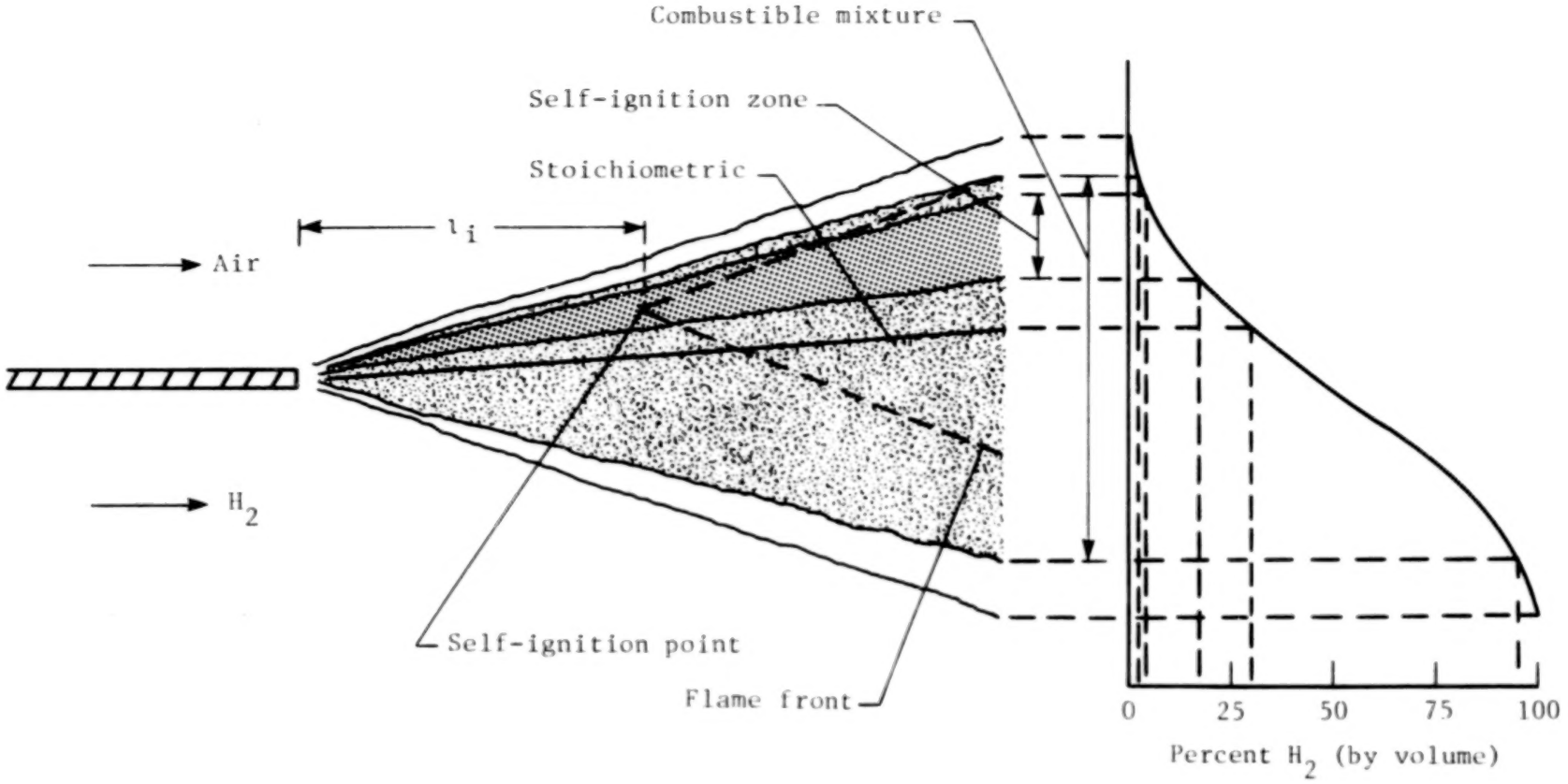

Figure 5.- Self-ignition in a supersonic parallel hydrogen-air mixing layer.

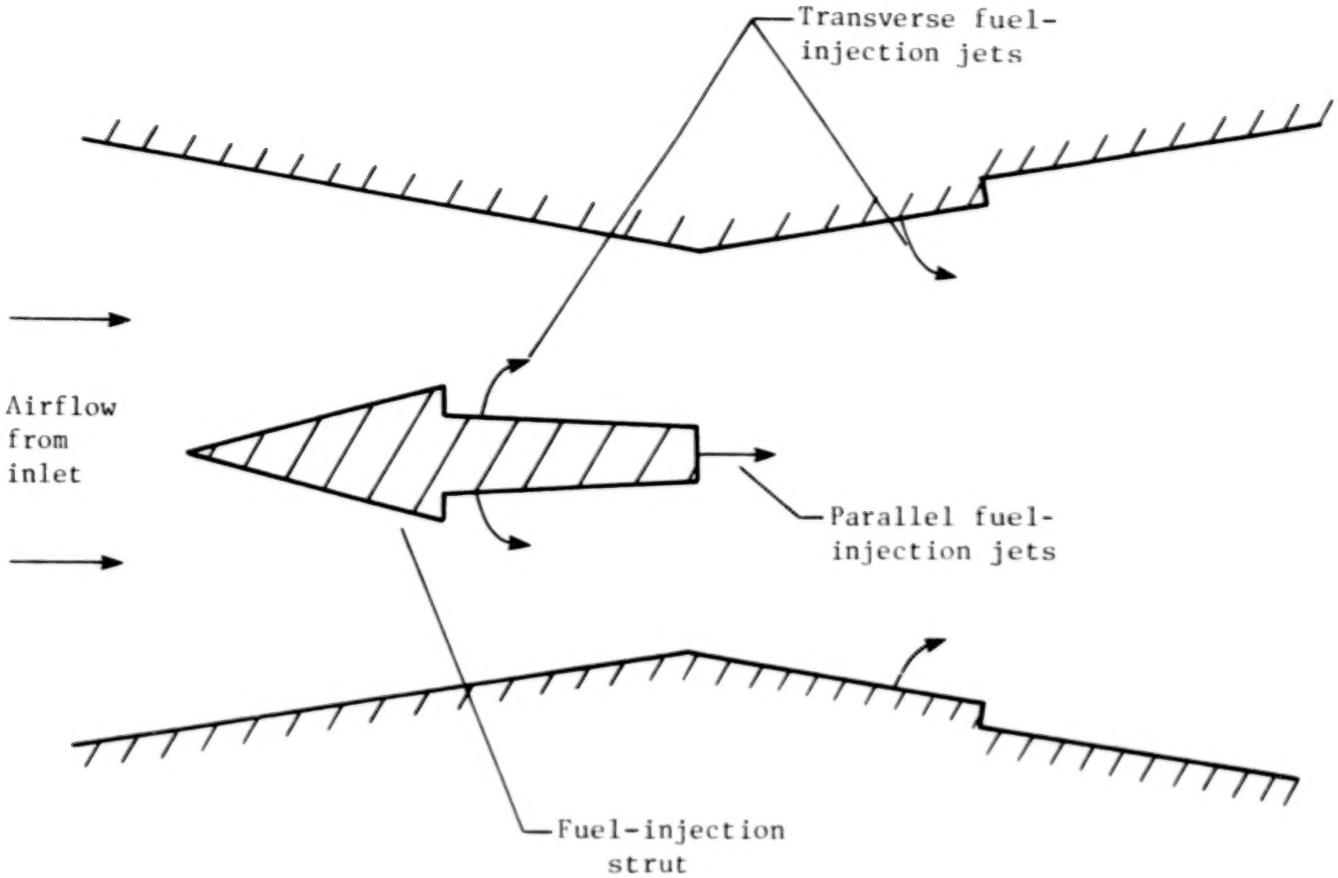

Figure 6.- Probable self-ignition points in a scramjet combustor.

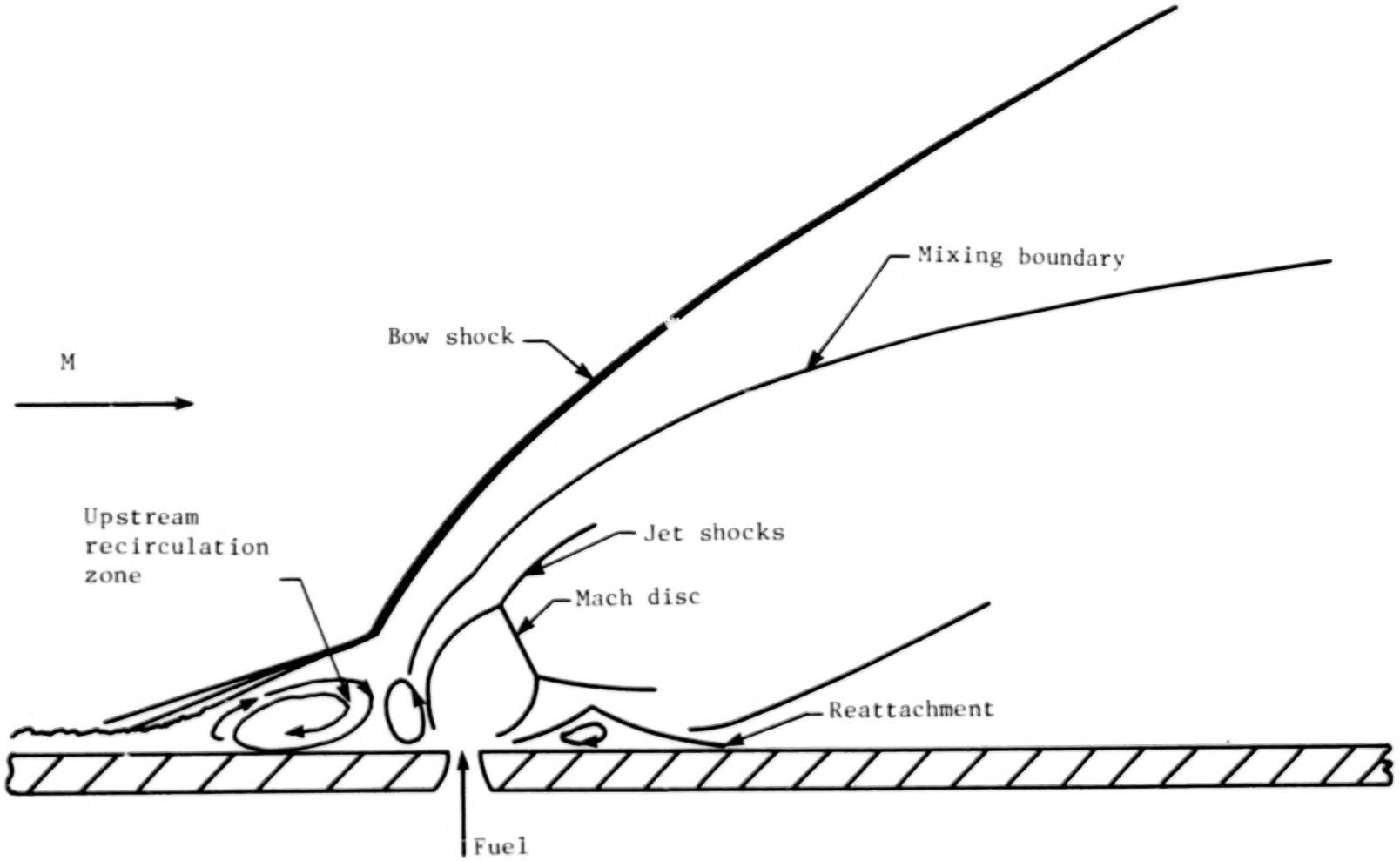

Figure 7.- Transverse fuel-injection flowfield.

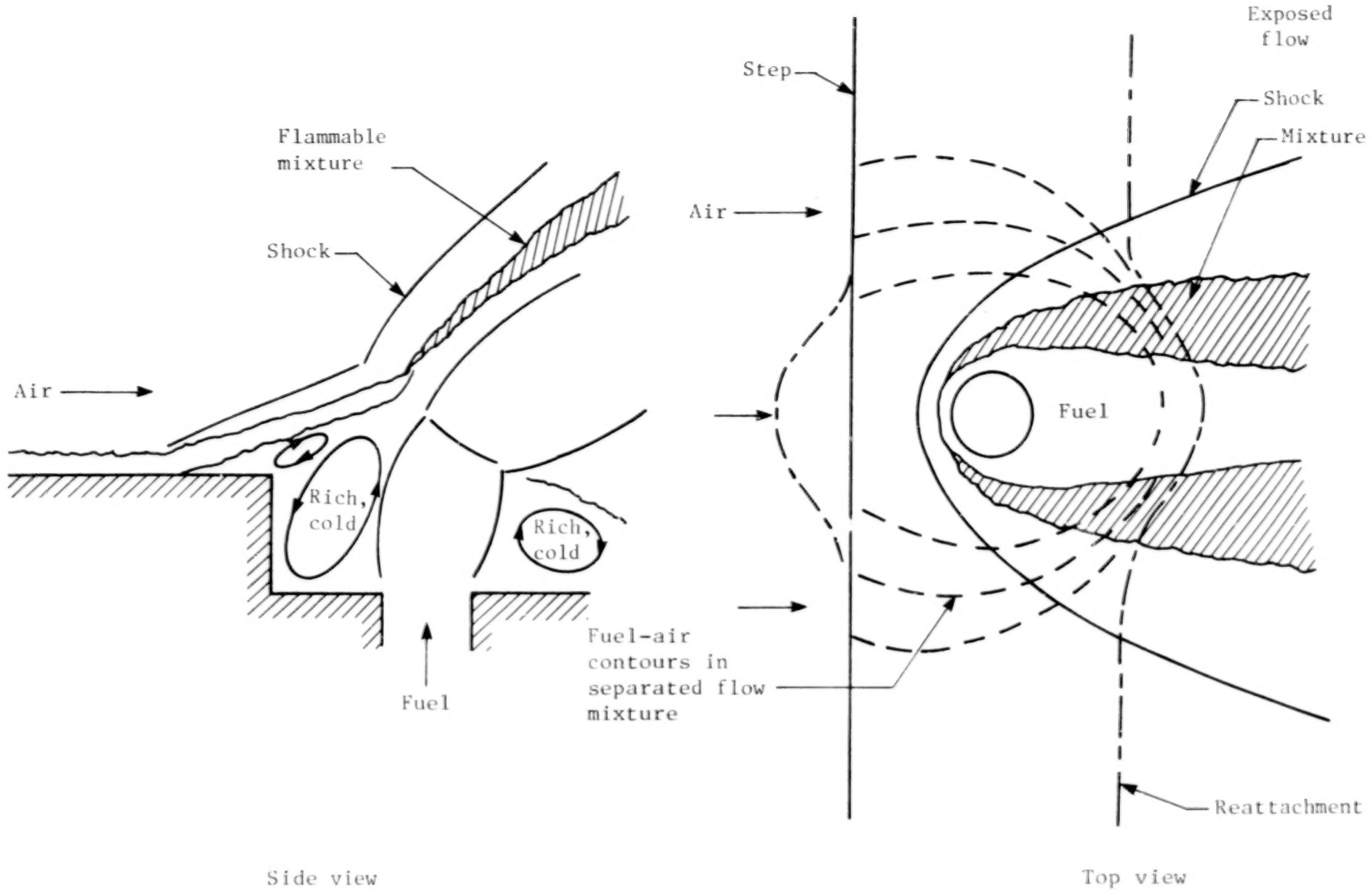

Figure 8.- Transverse injection behind unswept steps.

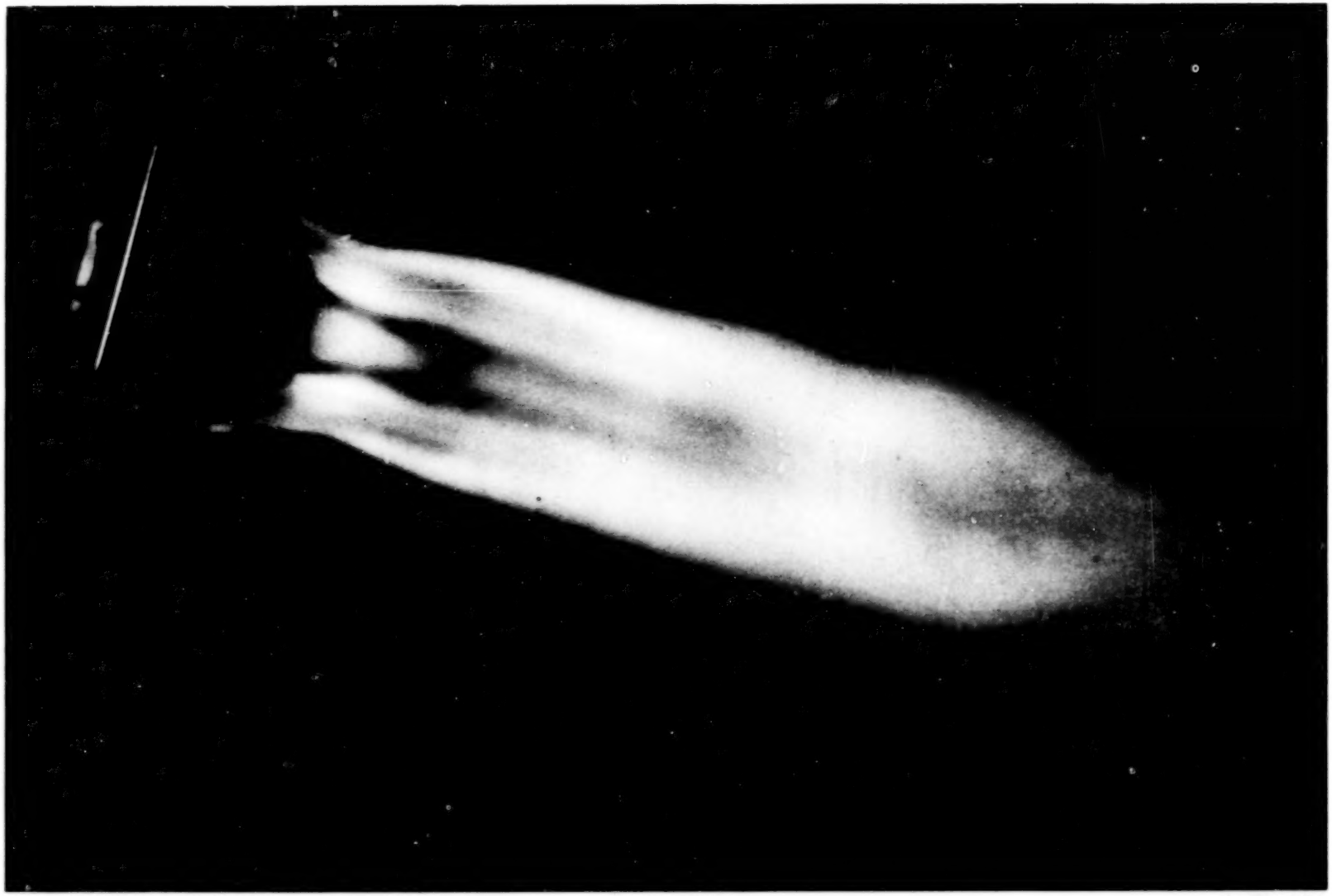

L-79-186

Figure 9.- Top view of transverse injection behind unswept step on strut.

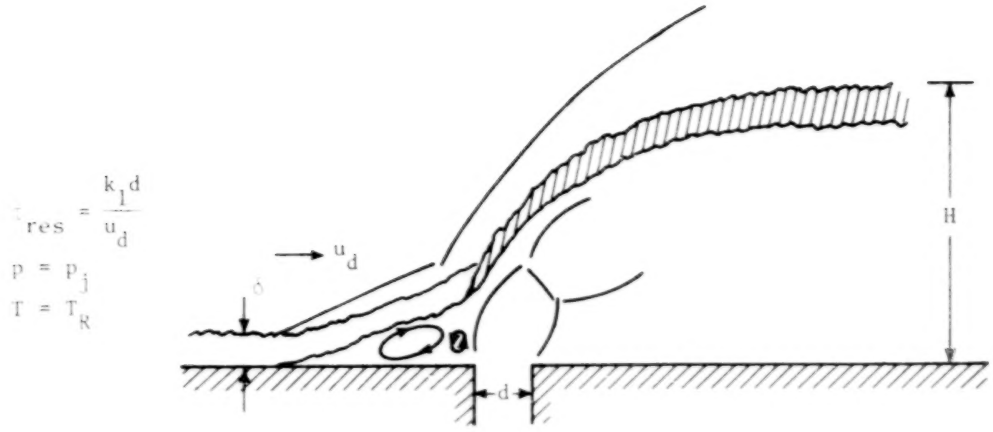

(a) Upstream recirculation model.

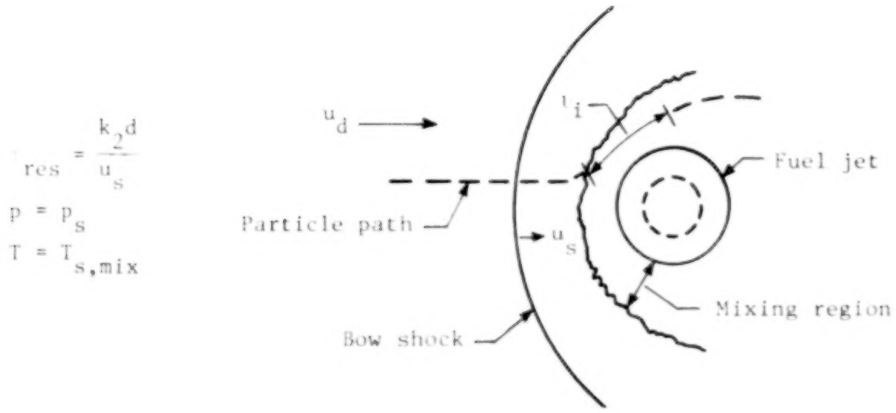

(b) Bow-shock model (top view).

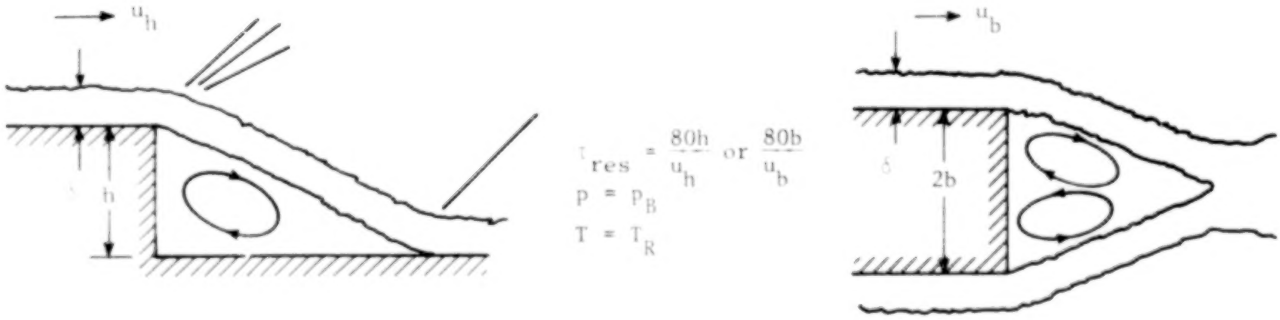

(c) Step and base models.

Figure 10.- Self-ignition models for transverse jet, step and base.

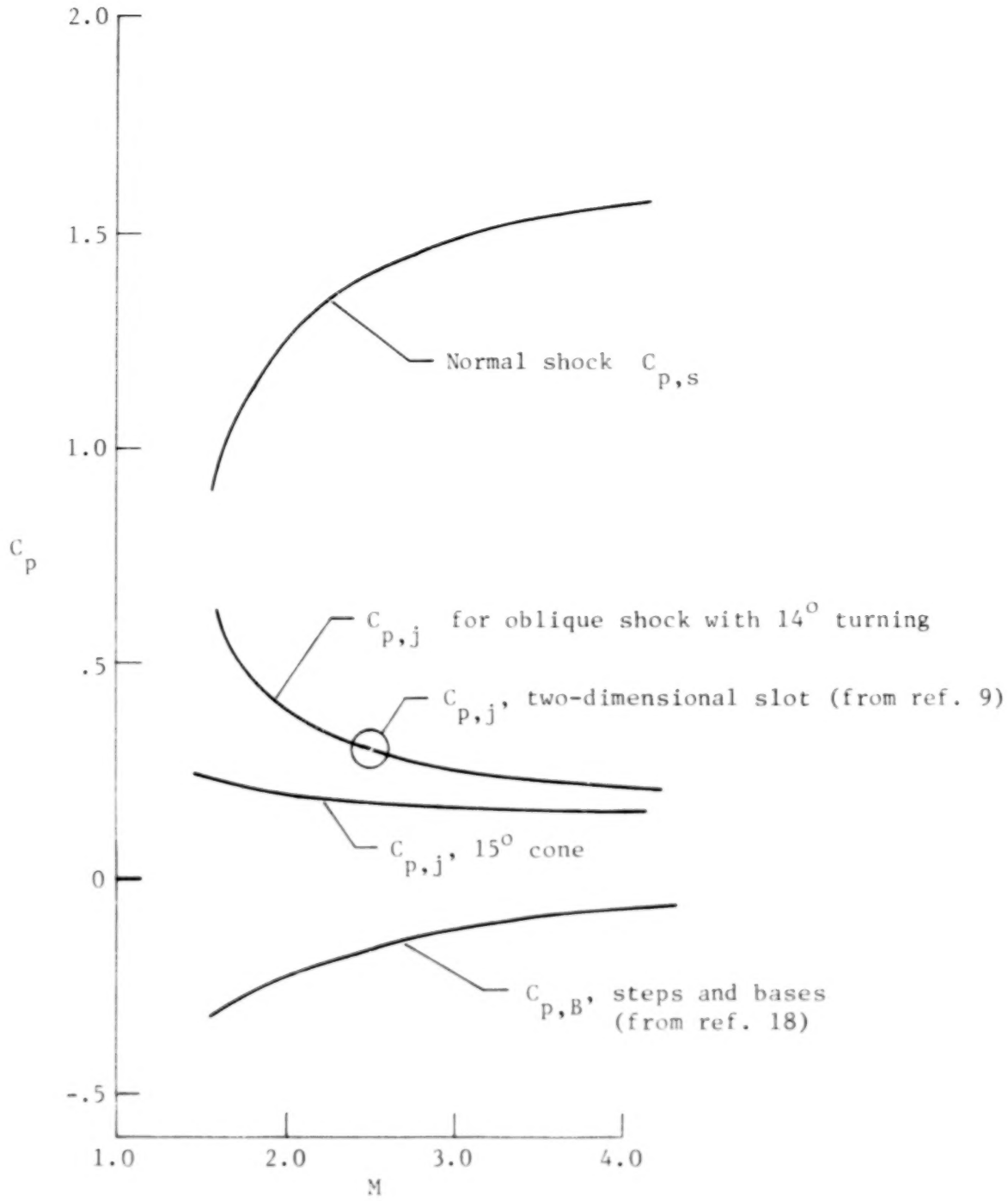

Figure 11.- Mach number dependency of pressure in recirculation zone ahead of transverse jets, behind jet bow shocks, and behind steps and bases.

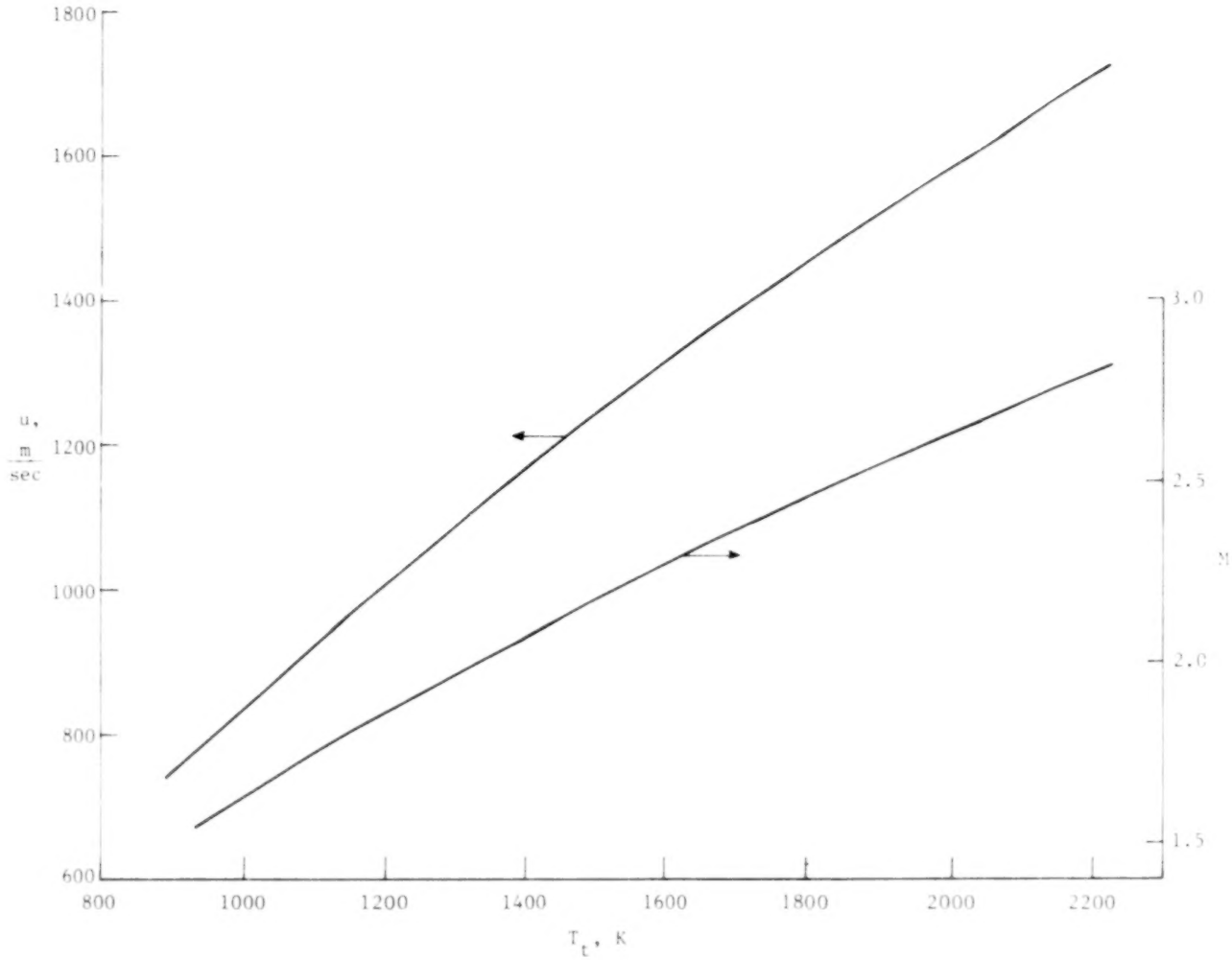

Figure 12.- Typical scramjet combustor entrance velocity and Mach number.

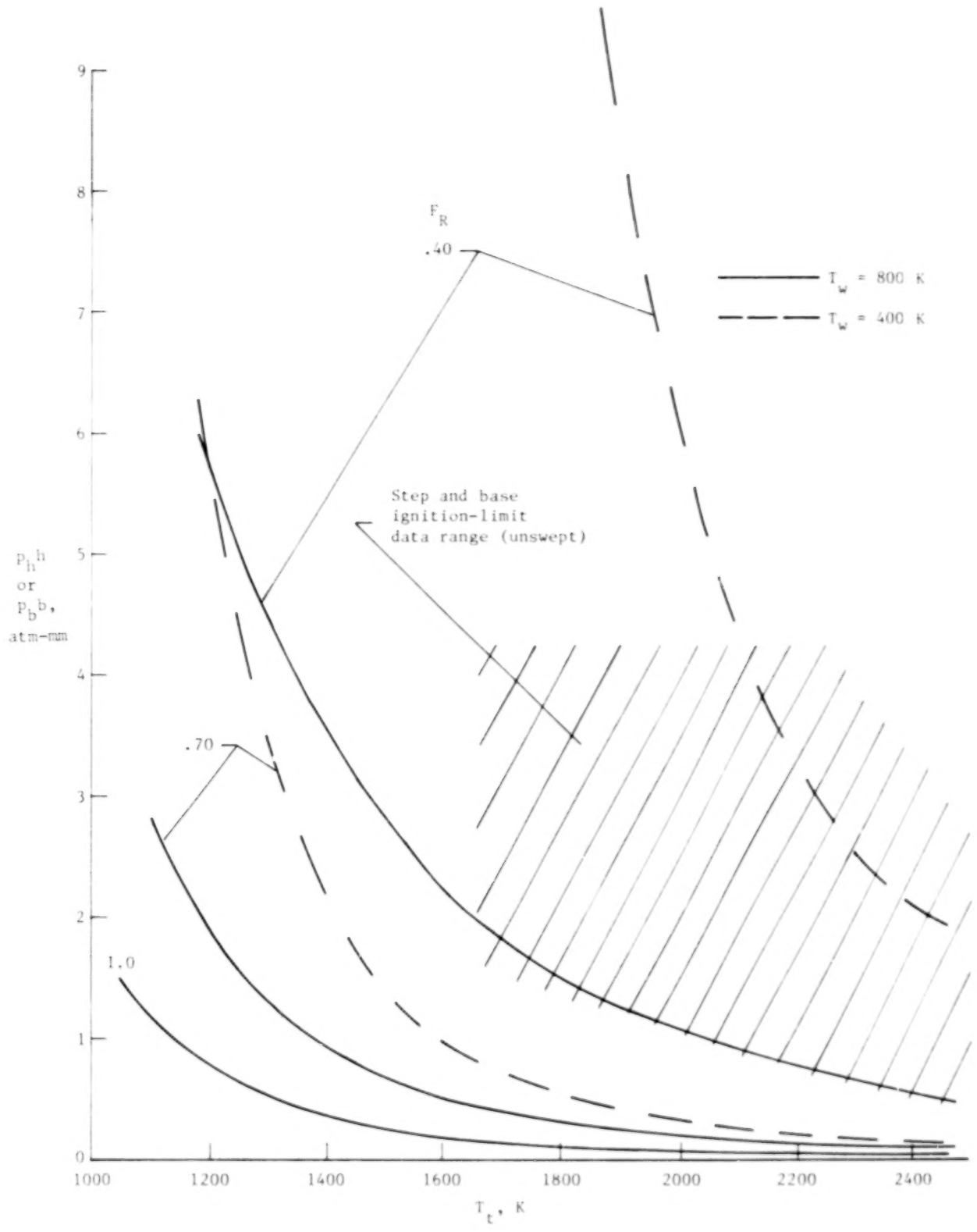

Figure 13.- Determination of best F_R for step and base ignition correlation.

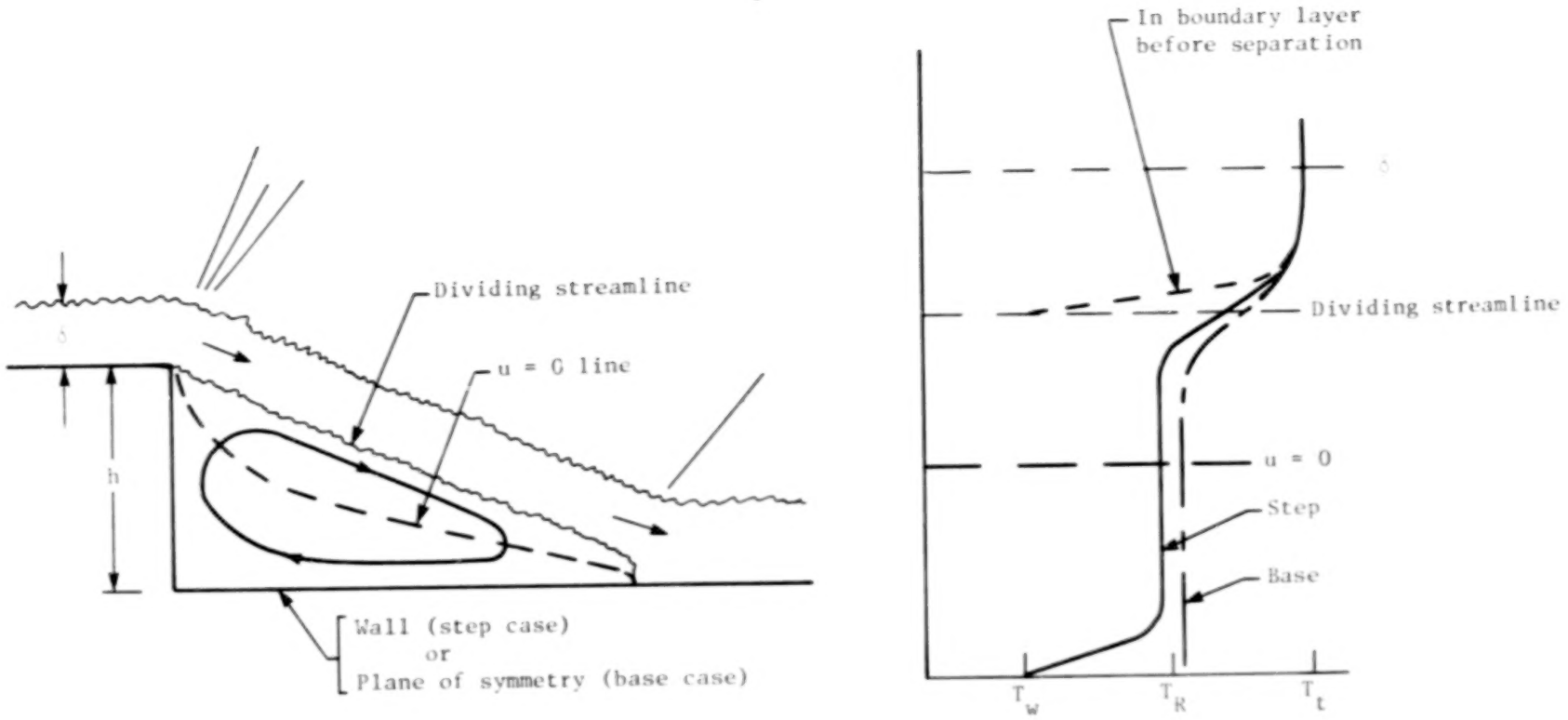

Figure 14.- Temperature profile in step and base recirculation zone.

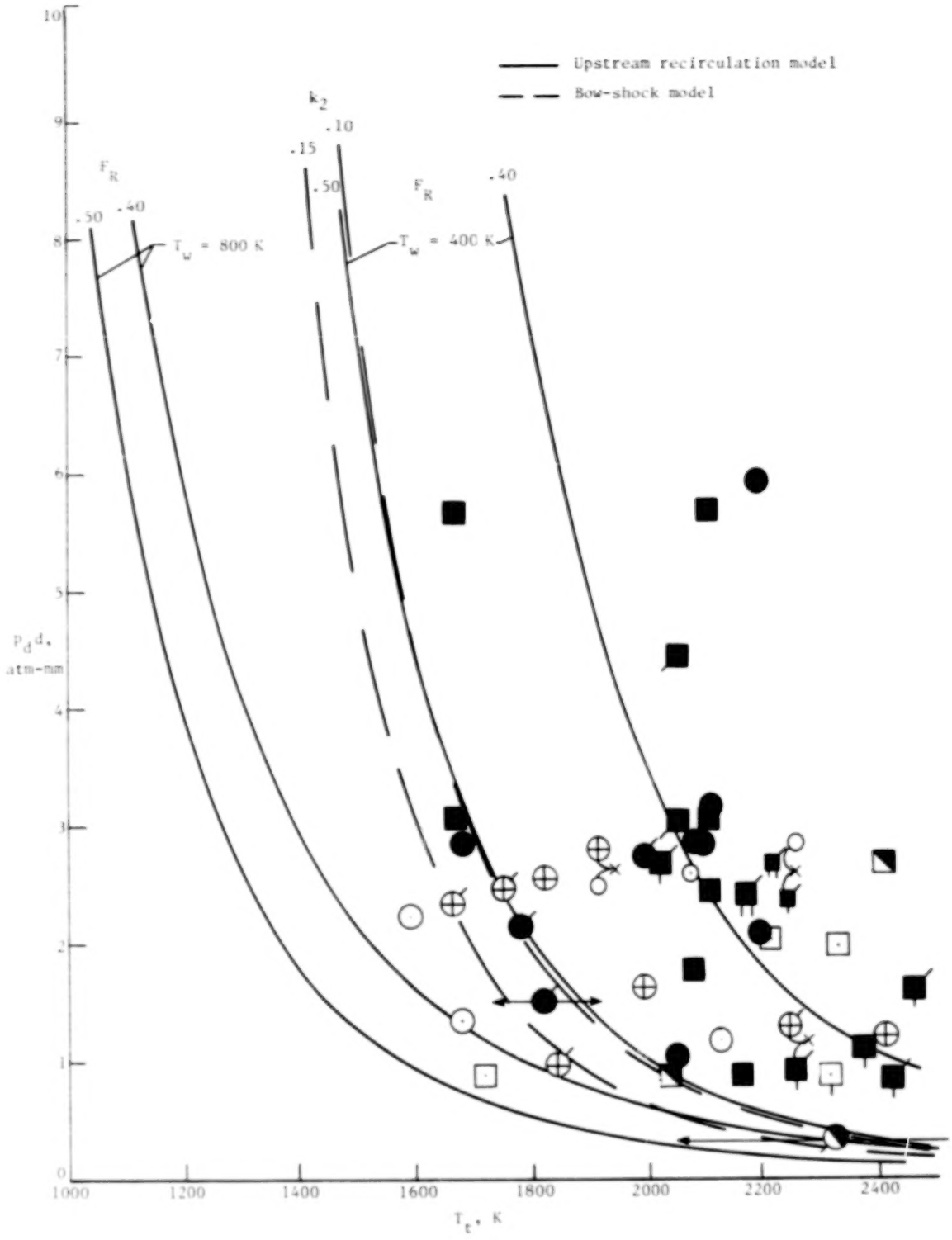

Figure 15.- Data correlation for transverse injectors (unswept). $k_1 = 20$. See table II for explanation of data symbols.

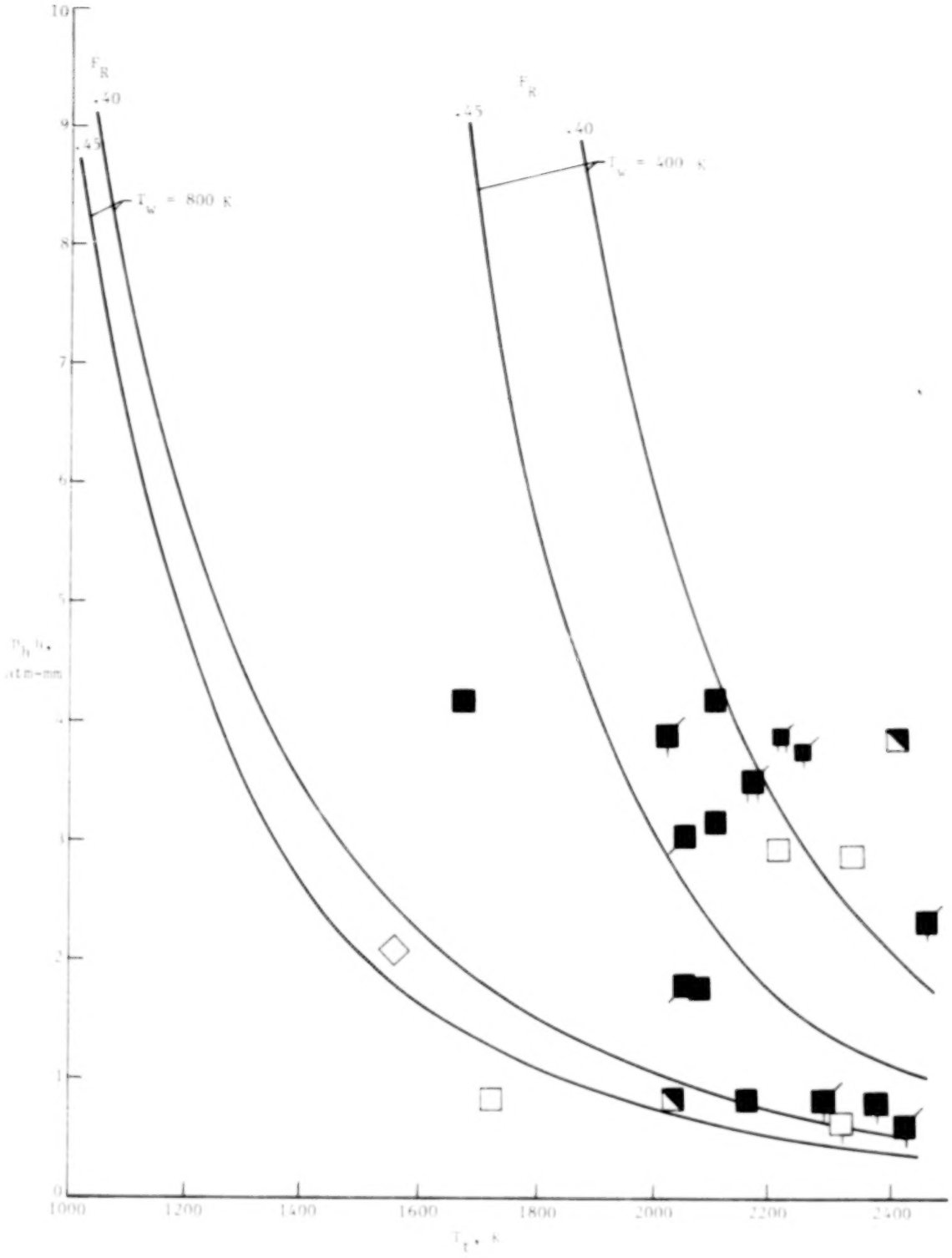

Figure 16.- Data correlation for rearward facing steps (unswept step model). See table II for explanation of data symbols.

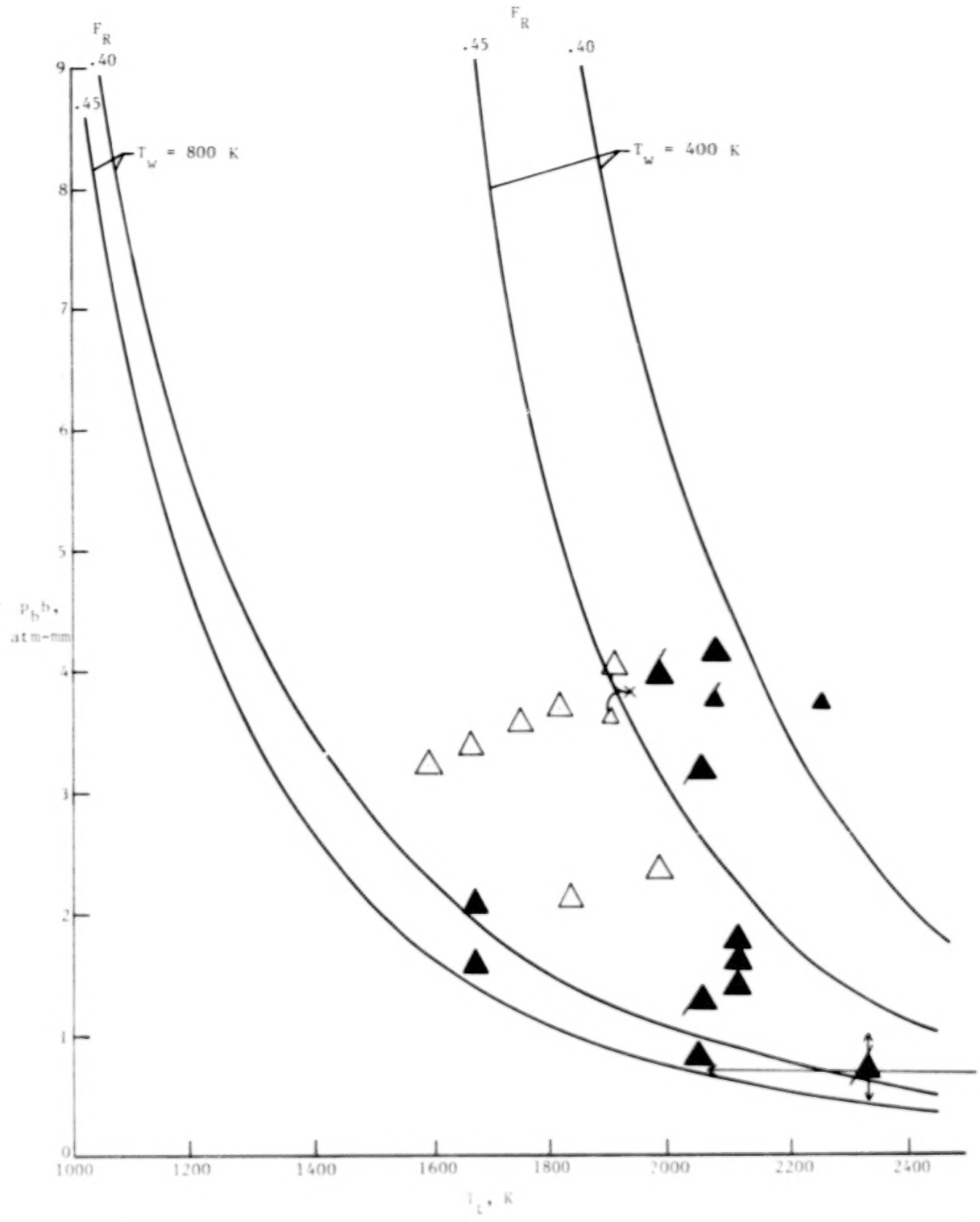

Figure 17.- Data correlation for bases (unswept base model). See table II for explanation of data symbols.

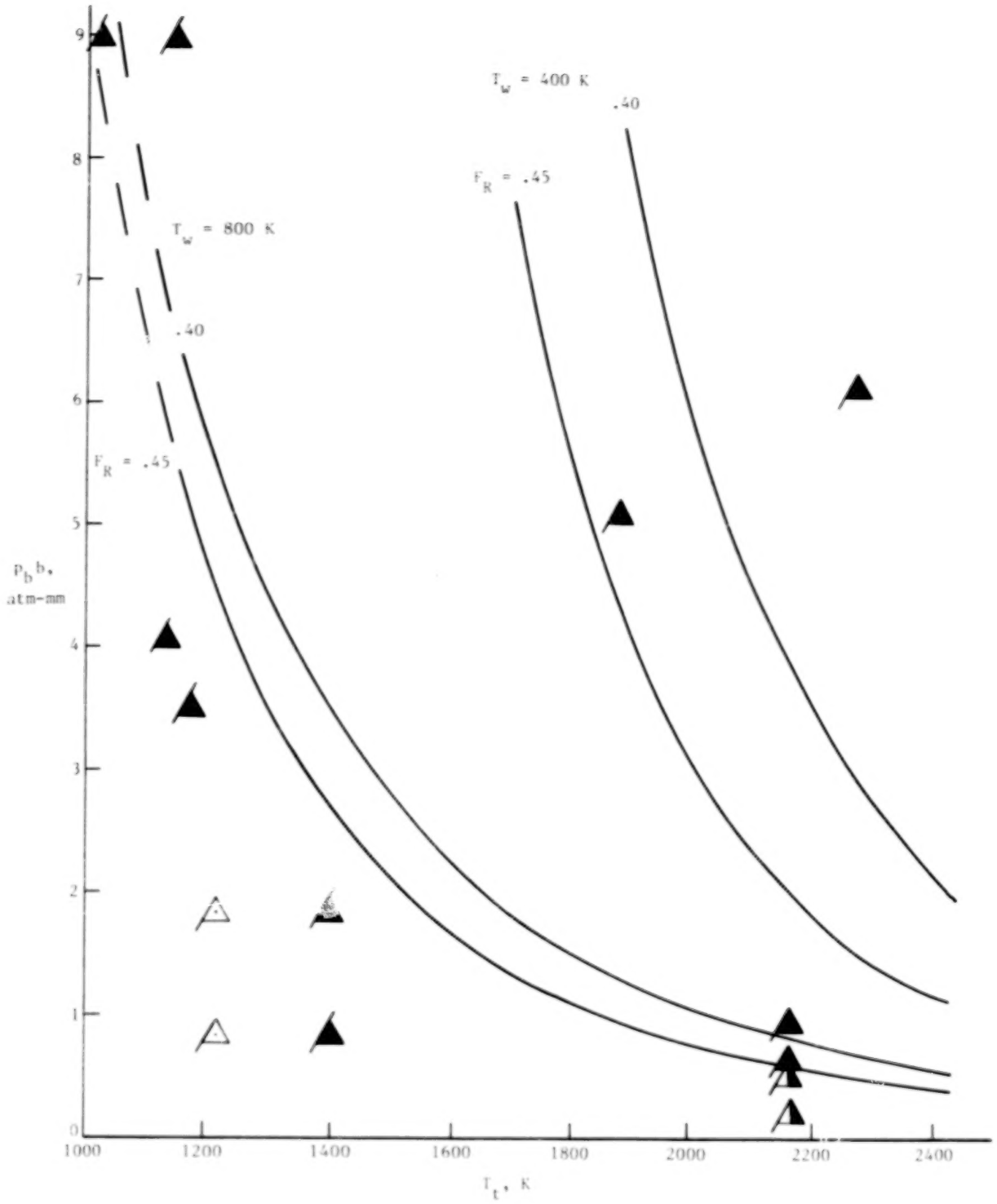

Figure 18.- Data correlation for strut bases (swept base model). See table II for explanation of data symbols.

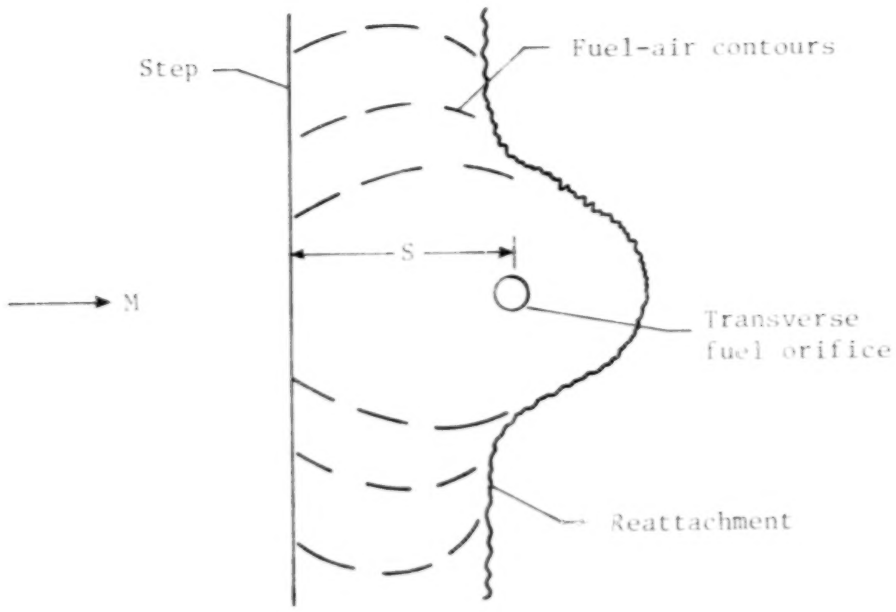

(a) Unswept case.

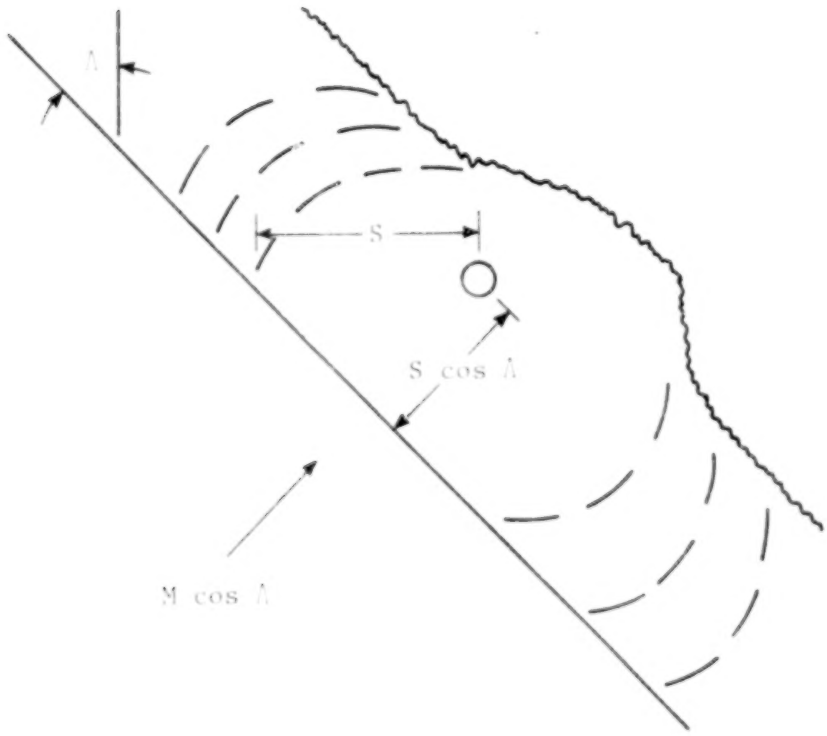

(b) Swept case.

Figure 19.- Schematic top view of recirculating zone behind unswept and swept steps.

1. Report No.	2. Government Accession No.	3. Recipient's Catalog No.
NASA TP-1457		

4. Title and Subtitle	5. Report Date
CRITERIA FOR SELF-IGNITION OF SUPERSONIC HYDROGEN-AIR MIXTURES	August 1979
	6. Performing Organization Code

7. Author(s)	8. Performing Organization Report No.
Paul W. Huber, Charles J. Schexnayder, Jr., and Charles R. McClinton	L-12678
	10. Work Unit No.
	505-05-43-01

9. Performing Organization Name and Address	11. Contract or Grant No.
NASA Langley Research Center Hampton, VA 23665	
	13. Type of Report and Period Covered
	Technical Paper

12. Sponsoring Agency Name and Address	14. Sponsoring Agency Code
National Aeronautics and Space Administration Washington, DC 20546	

15. Supplementary Notes

16. Abstract

A correlation of available self-ignition data for supersonic hydrogen-air mixtures in configurations representative of scramjet combustors has been made. The correlation was examined in light of simplified ignition-limit models. The data and model included cases of injection from transverse fuel jets on walls, transverse jets behind swept and unswept steps, and transverse injection ahead of swept and unswept steps and strut bases. The results provide useful guidance for predicting self-ignition in a variety of applications. The likely regions for self-ignition in a combustor are given in order of merit.

17. Key Words (Suggested by Author(s))	18. Distribution Statement
Ignition Hydrogen Supersonic combustion Scramjet engines Fuel injection	Unclassified - Unlimited Subject Category 07

19. Security Classif. (of this report)	20. Security Classif. (of this page)	21. No. of Pages	22. Price*
Unclassified	Unclassified	56	$5.25

* For sale by the National Technical Information Service, Springfield, Virginia 22161

NASA-Langley, 1979